

Astragaloside A Protects Against Photoreceptor Degeneration in Part Through Suppressing Oxidative Stress and DNA Damage-Induced Necroptosis and Inflammation in the Retina

Mei Li¹, Jing Xu^{1,2}, Yujue Wang¹, Xiaoye Du^{1,2}, Teng Zhang^{1,2}, Yu Chen¹⁻³

¹Yueyang Hospital of Integrated Traditional Chinese and Western Medicine, Shanghai University of Traditional Chinese Medicine, Shanghai, 200427, People's Republic of China; ²Clinical Research Institute of Integrative Medicine, Shanghai Academy of Traditional Chinese Medicine, Shanghai, 200437, People's Republic of China; ³Laboratory of Clinical and Molecular Pharmacology, Yueyang Hospital of Integrated Traditional Chinese and Western Medicine, Shanghai University of Traditional Chinese Medicine, Shanghai, 200427, People's Republic of China

Correspondence: Yu Chen, Yueyang Hospital of Integrated Traditional Chinese and Western Medicine, Shanghai University of Traditional Chinese Medicine, 110 Ganhe Road, Shanghai, 200437, People's Republic of China, Tel +86 21 5598 1009, Fax +86 21 5598 1009, Email chenyu@shutcm.edu.cn

Purpose: Photoreceptors are specialized retinal neurons responsible for phototransduction. Loss of photoreceptors directly leads to irreversible vision impairment. Pharmacological therapies protecting against photoreceptor degeneration are clinically lacking. Oxidative stress and inflammation are common mechanisms playing important roles in the pathogenesis of photoreceptor degeneration. Astragaloside A (AS-A) is a naturally occurring antioxidant and anti-inflammatory agent with neuroprotective activities. However, the photoreceptor protective effects of AS-A remain unknown. The current study thus aims to illustrate the pharmacological potentials of AS-A in protecting against photoreceptor degeneration.

Methods: BALB/c and C57/BL6J mice were exposed to bright light and DNA alkylating agent methyl methanesulfonate (MMS) to develop oxidative stress and DNA damage-mediated photoreceptor degeneration, respectively. Microstructural, morphological and functional assessments were performed to directly evaluate the photoreceptor protective effects of AS-A. Ultrastructural and molecular changes in the retina were examined to better understand the pharmacological mechanisms of AS-A in protecting against photoreceptor degeneration.

Results: AS-A protected against bright light-induced photoreceptor impairment. Bright light-induced retinal oxidative stress and photoreceptor cell death were attenuated by AS-A treatment. AS-A treatment mitigated bright light-induced DNA damage, activation of poly (ADP-ribose) polymerase (PARP) and nuclear dislocation of high mobility group box 1 (HMGB1) in photoreceptors. AS-A broadly counteracted bright light-altered retinal gene expression profiles. In particular, AS-A decreased the retinal expression of genes involved in necroptosis and inflammatory responses. Bright light-induced microglial activation was also suppressed as a result of AS-A treatment. Furthermore, AS-A attenuated MMS-induced photoreceptor morphological impairment, elevated expression of pro-necroptotic and proinflammatory genes as well as microglial activation in the retina.

Conclusion: The work here demonstrates for the first time that AS-A protects against photoreceptor degeneration in part through mitigating oxidative stress and DNA damage-induced necroptosis and inflammatory responses in the retina.

Keywords: retinal degeneration, photooxidative stress, photoreceptor protection, programmed cell death, microglial activation

Introduction

Photoreceptors are the first-order retinal neurons that carry out light detection and phototransduction functions, playing an essential role in initiating vision.¹ Photoreceptor degeneration is responsible for irreversible and progressive vision impairment in patients with age-related macular degeneration (AMD) and inherited retinal degeneration such as retinitis pigmentosa.^{2,3} A number of therapies have been evaluated in clinical trials and proven to be either ineffective or inconclusive regarding the efficacy to prevent the loss of photoreceptors in dry AMD. Ongoing clinical trials are also

available for the treatment of dry AMD. However, proper photoreceptor protective therapies have not been officially approved for clinical usage to prevent or delay the progression of photoreceptor degeneration.⁴

Photoreceptor degenerative disorders can be caused by mutations in the functional genes, environmental insults or a combination of both genetic and environmental factors. Regardless of the etiologies, programmed cell death triggered by oxidative stress is a common mechanism underlying the loss of photoreceptors.⁵ Moreover, photoreceptor degeneration is often accompanied and further aggravated by excessive inflammatory responses primarily mediated by activated microglial cells.⁶ Thus, suppressing photoreceptor cell death and mitigating retinal inflammation are equally important in the therapeutic management of photoreceptor degeneration.

Astragaloside A (AS-A), a triterpenoid saponin also known as astragaloside IV, is the major chemical component of *Astragalus membranaceus*, an herbal medicinal with a broad range of therapeutic effects including vision-enhancing properties in traditional Chinese medicine.⁷ Meanwhile, pharmacological studies have demonstrated that antioxidant and anti-inflammatory activities of AS-A contribute to the neuroprotective effects of AS-A observed in experimental models of Alzheimer's disease, Parkinson's disease and cerebral ischemia.^{7,8} However, whether AS-A is pharmacologically active in alleviating oxidative stress-mediated photoreceptor degeneration and associated retinal inflammation remains to be clarified. Therefore, in the current work, we tested the hypothesis that AS-IV may protect against photoreceptor degeneration by alleviating oxidative stress and inflammation in the retina.

Materials and Methods

Reagents

AS-A (purity >98%, Cat. No. B10462) was purchased from Shanghai Shifeng Biological Technology Co., Ltd (China). Methyl methanesulfonate (MMS) (Cat. No. 129925) was ordered from Sigma-Aldrich (USA).

Animal Treatment

BALB/c mice (female, 4–5 weeks of age, body weight averaging at 20±2 g), C57BL/6J mice (male, 6–8 weeks of age, body weight averaging at 22±2 g) were purchased from Shanghai Laboratory Animal Research Center (China). The mice were housed under controlled lighting (12/12h light/dark cycle), temperature (20±2°C) and humidity (35–55%) conditions with access to food and water *ad libitum*. The animal studies included in this work were reviewed and approved by the Institutional Animal Care and Use Committee, Yueyang Hospital of Integrated Traditional Chinese and Western Medicine, Shanghai University of Traditional Chinese Medicine (Approval No. YYLAC-2019-021-2). The animal handling procedures were carried out following the ARVO Statement for the Use of Animals in Ophthalmic and Vision Research. For experiments involving bright light exposure, BALB/c mice dark-adapted for 3 d were exposed to white light (LED Floodlight, 30W, PHILIPS) delivered at 15,000 lux for 30 min without dilation of the pupils. For examinations of the retinal structure and photoreceptor morphology, AS-A (dissolved in 30% DMSO in 0.9% saline solution) was administered at 6.25 mg/kg body weight (bw), 25 mg/kg bw and 100 mg/kg bw 30 min prior to light exposure via intraperitoneal injection. For the rest of the experiments, AS-A was administered at 100 mg/kg bw 30 min prior to light exposure via intraperitoneal injection. Mice unexposed to the indicated light and the light-exposed mice without AS-A treatment received vehicle treatment (30% DMSO in 0.9% saline solution) in the same manner. For the experiments involving MMS administration, C57BL/6J mice received intraperitoneal injection with MMS (dissolved in 0.9% saline solution) at the dose of 55 mg/kg body weight (bw). MMS-challenged mice received vehicle (0.9% saline solution) or AS-A treatment at 100 mg/kg bw via intraperitoneal injection twice a day until the experiment was terminated for the indicated analyses. C57/BL6J mice without MMS injection were treated with 0.9% saline solution to serve as the vehicle-treated normal controls.

Optical Coherence Tomography (OCT) Assessment

Image-guided OCT (OCT 2 with Micron IV, Phoenix Research labs, USA) was adopted to scan the retinal structure as previously described.⁹ Briefly, intraperitoneal injection of ketamine hydrochloride (82.5 mg/kg bw) and xylazine (8.25 mg/kg bw) was performed to induce anesthesia in the mice subject to OCT imaging, followed by dilation of pupils using 1% tropicamide. Five to ten full-retinal scans were acquired and averaged using Phoenix Reveal OCT software (Phoenix Research labs, USA).

Electroretinography (ERG) Recording

ERG was recorded under dim red light and analyzed with the universal testing and electrophysiological Ganzfeld system (Phoenix Research labs, USA) as previously described.⁹ In brief, dark-adapted mice were anesthetized with a mixture of ketamine hydrochloride (82.5 mg/kg bw) and xylazine (8.25 mg/kg bw). Scotopic ERGs were generated with flashes of green light at the intensities ranging from $-2 \log \text{cd.s.m}^{-2}$ to $3.1 \log \text{cd.s.m}^{-2}$.

Histological Examination and Immunohistochemistry (IHC)

For histological examination of the gross retinal morphology, enucleated eyeballs were fixed in 4% paraformaldehyde for 24h, followed by tissue processing for paraffin embedding. Paraffin sections were then cut at 4 μm and stained with hematoxylin and eosin (HE). For IHC purposes, paraffin sections were incubated with primary antibodies including mouse anti-rhodopsin (1:1000, NBP2-25160, Novus, USA), rabbit anti-M-opsin (1:100, AB5405, Millipore, USA), rabbit anti-S-opsin (1:100, AB5407, Millipore, USA), rabbit anti-protein kinase C α (PKC α) (1:5000, P4334, Sigma-Aldrich, USA), rabbit anti-calbindin D (1:1000, ab11426, Abcam, USA), rabbit anti-high mobility group box protein 1 (HMGB1) (1:1000, ab18256, Abcam, USA), rabbit anti-gamma H2A.X (γ H2AX) (phospho S139) (1:1000, ab81299, Abcam, USA), rabbit anti-SOD2 (1:500, D3X8F, Cell Signaling Technology, USA), rabbit anti-glutathione peroxidase 4 (GPX4) (1:200, ab125066, Abcam, USA), rabbit anti-bassoon (1:200, D63B6, Abcam, USA), rabbit anti-heat shock protein 60 (HSP60) (1:200, ab46789, Abcam, USA), mouse anti-Lamin B1 (1:500, sc-374015, Santa Cruz, USA). Cryosections were also prepared for IHC assessment. In brief, eye cups were dissected free of cornea and lens, fixed in 4% paraformaldehyde for 30 min at room temperature and processed for cryosectioning. Cryosections in the thickness of 12 μm were then incubated with the indicated primary antibodies including anti-ionized calcium binding adaptor molecule 1 (Iba1) (1:500, 019-19741, FUJIFILM Wako Pure Chemical Corporation, Japan) and mouse anti-poly (ADP-ribose) (PAR) (1:1000, ALX-804-220-R100, Enzo Life Sciences, USA). Secondary antibodies used for IHC examinations included Cy3-conjugated sheep anti-mouse antibody (1: 1000, C2181, Sigma-Aldrich, USA), Cy3-conjugated sheep anti-rabbit antibody (1: 1000, C2036, Sigma-Aldrich, USA) and Alexa Fluor 488-conjugated donkey anti-rabbit antibody (1:500, ab150073, Abcam, USA). Nuclear counterstaining was performed using 4',6-diamidino-2-phenylindole (DAPI) (D8200, ROCHE, USA). After HE staining, the retinal morphology was examined and recorded by a light microscope (DM2000, Leica, Germany). After the indicated IHC examinations, images were observed and recorded using a fluorescent microscope (DM6000B, Leica, Germany). Leica LAS AF software was used to acquire fluorescence images. The camera gain and exposure time for each indicated staining were kept the same across all experimental groups. The immunopositivity of the indicated immunostaining was analyzed using ImageJ. For each section, at least four images from the superior, inferior and central retina were obtained.

Transmission Electron Microscopy (TEM) Assessment

The eyeballs were quickly removed and fixed in pre-cooled 2.5% glutaraldehyde phosphate buffer at 4°C for 2h. The lens and cornea were then removed from the eyeballs to make eye cups. The eye cups at the temporal side of the optic disc were cut into strips in the size of approximately 1 mm \times 2 mm, followed by fixation in pre-cooled 2.5% glutaraldehyde phosphate buffer at 4°C overnight. The tissue strips were then rinsed in PBS, fixed with 1% osmium tetroxide at 4°C for 2h, dehydrated, stained en bloc by 3% uranyl acetate and embedded in EPON. Ultrathin sections were made using an ultramicrotome (Leica EM UC7, Leica Microsystems, Germany) and stained with lead citrate. The ultrastructure of the retina was then observed using a transmission electron microscope (H-7650, Hitachi, Japan).

In situ Detection of Reactive Oxygen Species (ROS) in the Retina

In situ detection of superoxide formation was performed as previously described.^{9,10} In brief, superoxide probe dihydroethidium (DHE) (Sigma-Aldrich, USA) was intraperitoneally administered at the dose of 20 mg/kg bw. Eye cups were made 2h after DHE administration and fixed in 4% paraformaldehyde for 30 min, followed by processing for cryosectioning. Cryosections 12 μm thick were counterstained with DAPI and imaged using a fluorescent microscope (DM6000B, Leica, Germany). At least 4 fluorescence images were acquired from the superior, inferior and central retina

of each section using Leica LAS AF software with the same camera gain and exposure setup for all experimental groups. The positivity of DHE was analyzed using ImageJ.

TdT-Mediated dUTP Nick-End Labeling (TUNEL) Assay

In situ detection of cell death in the retina was performed by a TUNEL assay. Paraffin sections made from the enucleated eyes after the indicated treatments were subject to TUNEL assessment following the manufacturer's instructions (DeadEnd™ Fluorometric TUNEL system, Promega, USA). Images were observed using a fluorescent microscope (DM6000B, Leica, Germany). At least 4 fluorescence images were captured from the superior, inferior and central retina of each section using Leica LAS AF software. The camera gain and exposure time were kept the same for all experimental groups. The TUNEL positivity was analyzed using ImageJ.

RNA-Seq Analysis

Total RNA was isolated from the mouse retina using a mirVana miRNA Isolation Kit (Thermo Fisher Scientific, USA) following the manufacturer's protocols. The purity and the amount of RNA were evaluated using a NanoDrop 2000 spectrophotometer (Thermo Fisher Scientific, USA). RNA integrity was assessed using an Agilent 2100 Bioanalyzer (Agilent Technologies, USA). The cDNA libraries were constructed using a TruSeq Stranded mRNA LT Sample Prep Kit (Illumina, San Diego, CA, USA) following the manufacturer's instructions. Libraries were sequenced on an Illumina NovaSeq 6000 platform. Raw data in the fastq format were processed using Trimmomatic¹¹ and the low-quality reads were removed. The clean reads were then mapped to reference genome using hisat2.¹² FPKM value of each gene was calculated using cufflinks¹³ and the read counts of each gene were obtained by htseq-count.¹⁴ Distribution and variation of the samples were evaluated by principal component analysis (PCA). Differentially expressed genes (DEGs) were identified using the *DESeq2* R Package functions estimateSizeFactors and nbinomTest.¹⁵ Significantly differential expression was defined as P value<0.05 and fold change>1.5. Hierarchical cluster analysis of DEGs was performed to demonstrate the expression pattern of genes in the indicated treatment groups. To perform functional enrichment analysis, the gene set enrichment analysis (GSEA) based on Kyoto Encyclopedia of Genes and Genomes (KEGG) and Gene Ontology (GO) gene sets were carried out using *ClusterProfiler* R package and org.Mm.eg.db annotation package.¹⁶ The gene sets with absolute value of normalized enrichment score (NES)>1 and false discovery rate (FDR) q-value<0.05 were considered as significantly enriched. The related FDR q-value was corrected using the Benjamini-Hochberg procedure.

Real-Time Quantitative PCR (qPCR) Analysis

Total RNA was isolated from the mouse retina using TRIzol reagent (Invitrogen, USA), followed by reverse transcription using PrimeScript RT Master Mix (TaKaRa, Japan). The mRNA expression of *Ccl2*, *Ccl3*, *Ccl4*, *Cd68*, *Fas*, *Il1b*, *Mkl1*, *Ripk1*, *Ripk3*, *Tlr2*, *Tlr4*, *Tnf*, *Tspo* and *Zbp1* was analyzed using LightCycler 480 SYBR Green I Master (Roche, Germany) on a LightCycler 480 II system (Roche, USA). 18s rRNA was analyzed in parallel for normalization purposes. The primer sequences were included in [Supplementary Table 1](#). The fold change in the gene expression was calculated according to $2^{-[Ct(\text{candidate}) - Ct(18s\ rRNA)]}$.

Statistical Analysis

The data were presented as mean±standard error of mean (S.E.M). The statistical analyses were performed by Student's *t*-test or one-way ANOVA with the Turkey multiple-comparisons test. Statistical significance was defined as P<0.05.

Results

AS-A Alleviates Photooxidative Stress-Mediated Photoreceptor Microstructural and Morphological Impairment

Oxidative stress is a central mechanism mediating photoreceptor degeneration. Bright light exposure induces photooxidative stress in photoreceptors and is commonly adopted to experimentally recapitulate photoreceptor degenerative pathologies in vivo.¹⁷ To directly assess the photoreceptor protective properties of AS-A, bright light exposure was

applied to BALB/c mice to induce photooxidative stress-mediated photoreceptor degeneration. AS-A was administered to the light-exposed mice at the doses of 6.25 mg/kg bw, 25 mg/kg bw and 100 mg/kg bw. Vehicle-treated mice with and without bright light exposure served as the vehicle and normal controls, respectively. OCT imaging was performed to obtain full-retinal cross-sectional scans for the non-biased assessment of the retinal microstructure. As shown in Figure 1A, the microstructure of photoreceptors including outer nuclear layer (ONL), outer segment (OS) and inner segment (IS) was severely impaired in the light-exposed vehicle-treated mice, while the microstructure of the inner retina remained largely unaffected. A partial preservation of the photoreceptor microstructure in the inferior and superior retina was observed when AS-A was administered at 6.25 and 25 mg/kg bw. A nearly complete protection of the photoreceptor microstructure was observed in both the inferior and superior retina in the light-exposed mice treated with 100 mg/kg bw AS-A. Measurement of the thickness of ONL and OS/IS in the superior (Figure 1B) and inferior (Figure 1C) retina consistently showed that the ONL and OS/IS were much thinner in the light-exposed vehicle-treated retina compared to that from the normal controls, whereas AS-A treatment resulted in significantly thicker ONL and OS/IS compared to that from the light-exposed vehicle-treated retinas (Figure 1B and C).

Histological assessment was further performed to examine the retinal morphological changes in detail. As shown in Figure 2A, in distinct contrast to the intact morphology of OS and IS observed in the normal controls, the OS and IS were nearly undetectable in the light-exposed vehicle-treated retinas. The ONL was organized into 11–13 rows of neatly

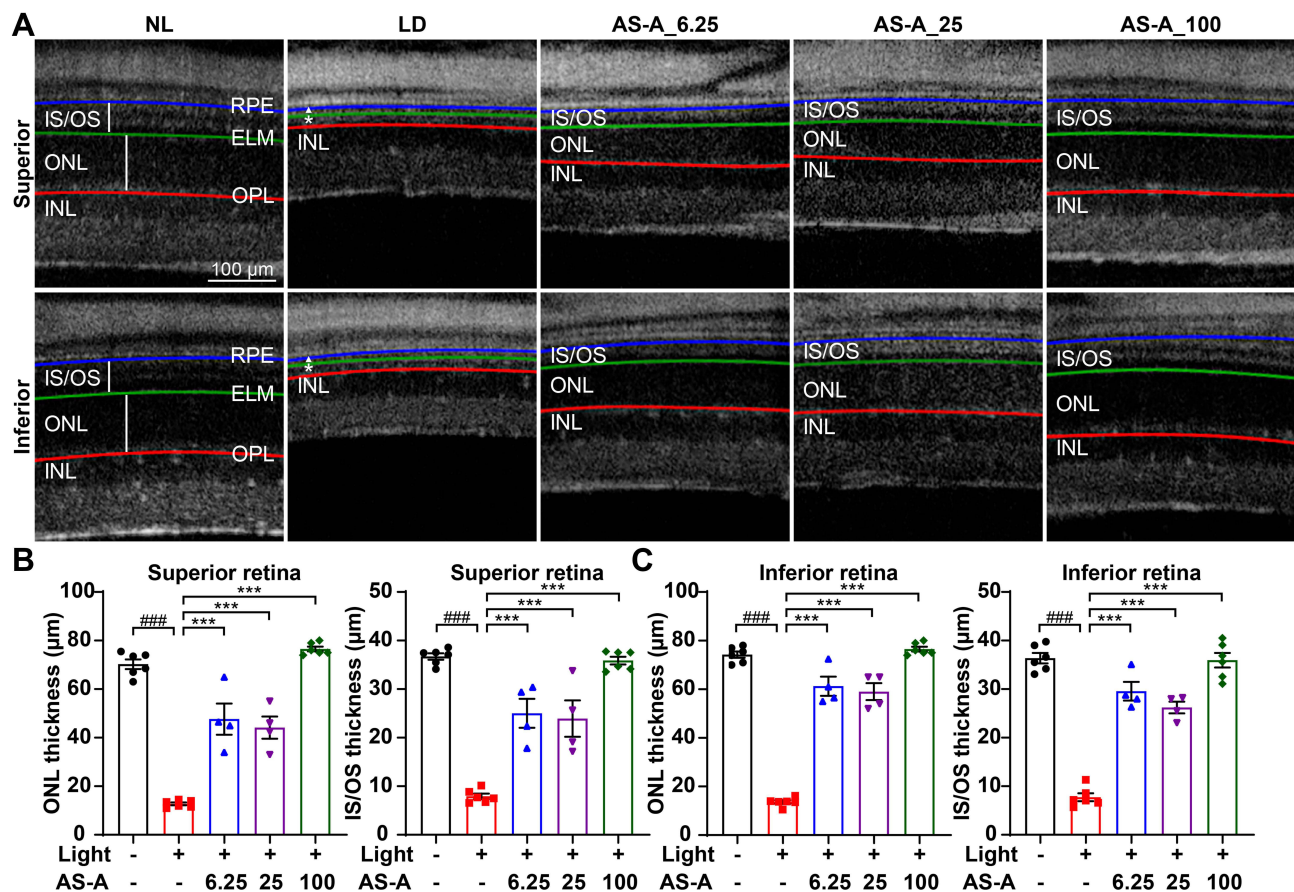


Figure 1 AS-A protects against bright light-induced microstructural impairment of photoreceptors. Vehicle (LD) or AS-A was administered 30 min prior to exposing the dark-adapted BALB/c mice to white light at 15,000 lux for 30 min. AS-A was administered at 6.25 mg/kg bw (AS-A_6.25), 25 mg/kg bw (AS-A_25) and 100 mg/kg bw (AS-A_100). Dark-adapted BALB/c mice without the indicated light exposure received vehicle treatment in the same manner (NL). (A) Seven days after the light exposure, OCT imaging was performed to scan the retinal microstructure. (B and C) The thickness of ONL and OS/IS was measured at 500 µm off the ONH in the superior and inferior retina, respectively. White asterisk and closed triangle point to impaired ONL and IS/OS, respectively. Data were expressed as mean±S.E.M (n=4-6 per group). ### Compared to that from NL, P<0.001; *** compared to that from LD, P<0.001.

Abbreviations: ELM, external limiting membrane (green line); INL, inner nuclear layer; IS, inner segment; ONL, outer nuclear layer; OPL, outer plexiform layer (red line); OS, outer segment; RPE, retinal pigment epithelium (blue line).

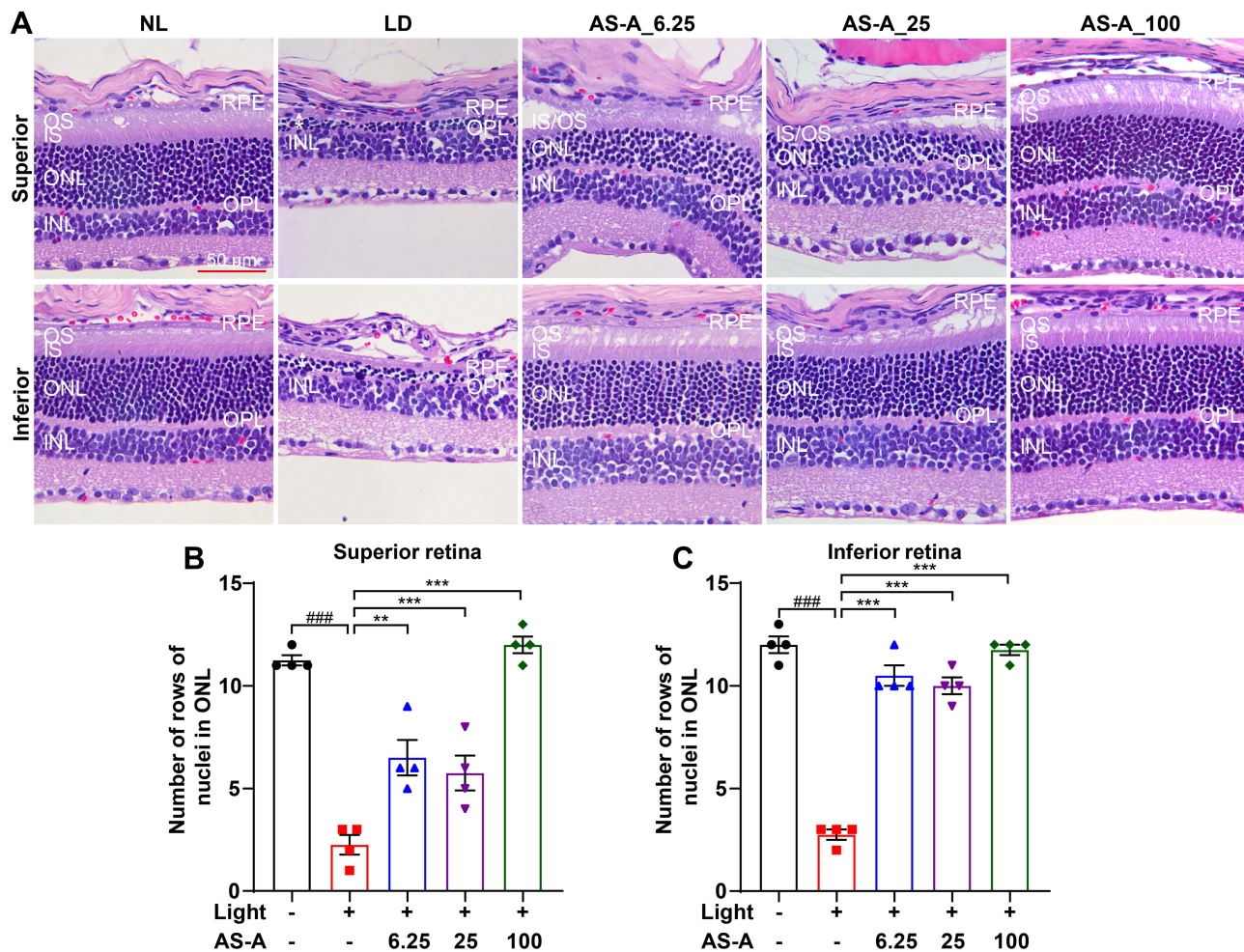


Figure 2 AS-A protects against bright light-induced morphological impairment of photoreceptors. Eyes were enucleated from the indicated treatment groups 7 d after bright light exposure. **(A)** Histological examination was performed by HE staining. Representative micrographs taken from the central retinas were presented. **(B and C)** Number of rows of nuclei in ONL was measured in the superior and inferior retina, respectively. White asterisk and closed triangle point to diminished ONL and IS/OS, respectively. Data were expressed as mean±S.E.M (n=4 per group). #### Compared to that from NL, P<0.001; ** compared to that from LD, P<0.01; *** compared to that from LD, P<0.001.

Abbreviations: INL, inner nuclear layer; IS, inner segment; ONL, outer nuclear layer; OPL, outer plexiform layer; OS, outer segment; RPE, retinal pigment epithelium.

aligned photoreceptor nuclei in the normal controls, whereas only 2–3 rows of photoreceptor nuclei remained in the light-exposed vehicle-treated retinas. However, in the light-exposed mice treated with 100 mg/kg bw AS-A, the morphology of the OS, IS and ONL was well-preserved. In the light-exposed mice treated with 6.25 and 25 mg/kg bw AS-A, improved morphology of the OS, IS and ONL, in particular that of the IS and ONL, was observed in the inferior retinas. Meanwhile, compared to that from the light-exposed vehicle-treated mice, the number of photoreceptor nuclei was significantly increased in both the superior (Figure 2B) and inferior retinas (Figure 2C) in the light-exposed mice treated with AS-A at all the doses. The results from OCT imaging and histological assessment collectively demonstrate that AS-A treatment is effective at protecting photoreceptors from developing photooxidative stress-induced microstructural and morphological degeneration.

AS-A Protects Against Photooxidative Stress-Induced Impairment of the Retinal Function

Next, ERG was performed to evaluate the pharmacological significance of AS-A in protecting against photooxidative stress-induced impairment of the retinal function. Given that a nearly complete protection of the photoreceptor

microstructure and morphology was observed when AS-A was administered at 100 mg/kg bw (Figures 1 and 2), the light-exposed BALB/c mice were treated with either vehicle or AS-A at 100 mg/kg bw in an independent experiment, followed by ERG analysis of the scotopic a-wave (Figure 3A and B) and b-wave (Figure 3A and C). The results showed that in contrast to distinct ERG responses of light intensity-dependent increases in the a-wave and b-wave amplitudes manifested by the normal controls, light intensity-dependent increases in the a-wave and b-wave amplitudes were markedly dampened in the light-exposed vehicle-treated mice. However, ERG responses similar to that observed in the normal controls were recorded in the light-exposed AS-A-treated mice, which exhibited significantly increased a-wave and b-wave amplitudes compared to that from the light-exposed vehicle-treated mice. Thus, the results from ERG recording demonstrate that AS-A is effective at preserving the retinal function under photooxidative stress conditions.

AS-A Maintains the Morphological Integrity of Photoreceptors and Second-Order Retinal Neurons Under Photooxidative Stress Conditions

Our previous work has demonstrated that in addition to triggering loss of photoreceptors, photooxidative stress also causes morphological impairment to the second-order retinal neurons such as bipolar cells and horizontal cells, which may collectively contribute to the impairment of the retinal function.^{18–22} Rhodopsin, M-opsin and S-opsin are function proteins marking rod, middle-wavelength and short-wavelength cone photoreceptors, respectively. The bipolar cells and horizontal cells are positive for PKC α and calbindin D, respectively. Thus, IHC examination was further performed to visualize the impact of AS-A treatment on the morphological integrity of rod photoreceptors, cone photoreceptors as well as the bipolar cells and horizontal cells. As shown in Figure 4A and B, abundant expression of rhodopsin was readily detected in the OS in the normal controls, while the expression of rhodopsin was markedly diminished in the light-exposed vehicle-treated retinas. The expression of M-opsin (Figure 4C and D) and S-opsin (Figure 4E and F) was also diminished in the light-exposed vehicle-treated retina compared to that from the normal

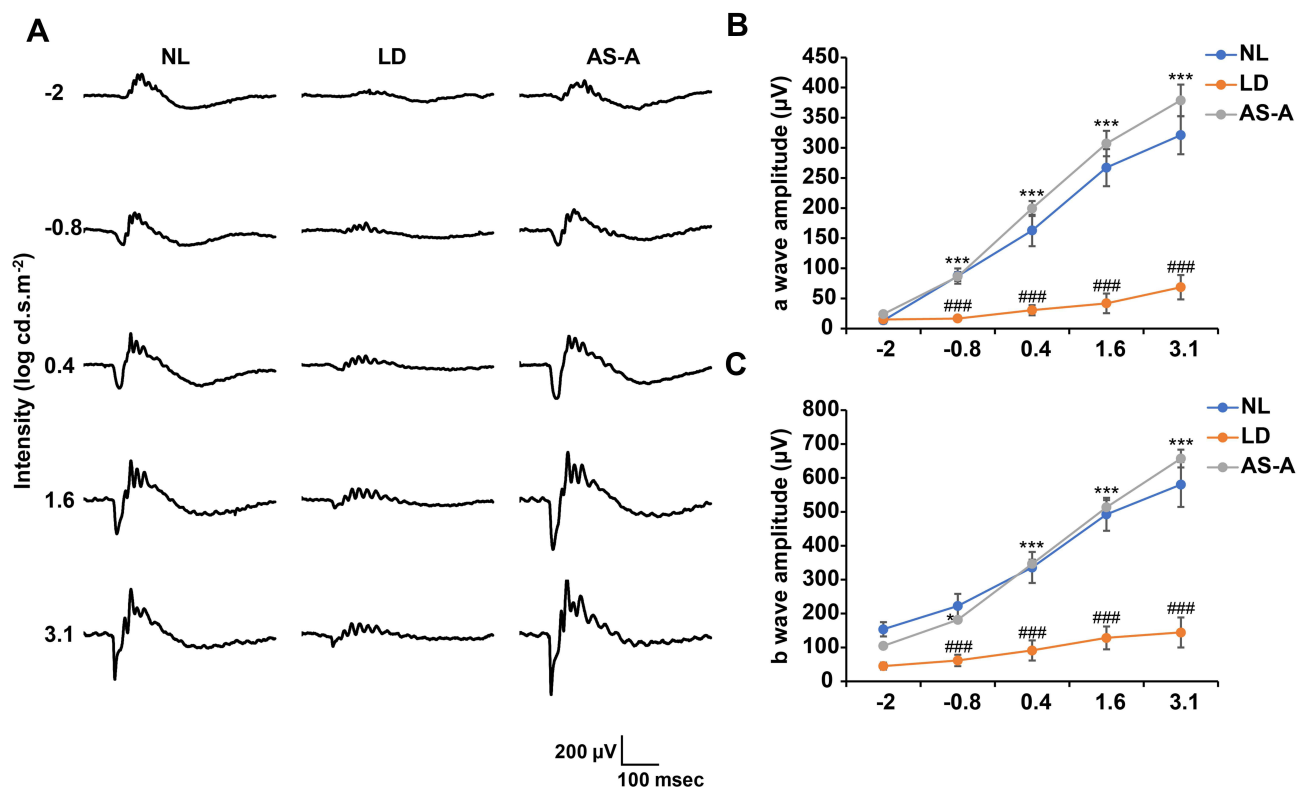


Figure 3 AS-A protects against bright light-induced impairment in the retinal function. Dark-adapted BALB/c mice were treated with vehicle (LD) or AS-A at 100 mg/kg bw (AS-A) 30 min prior to the light exposure. Dark-adapted BALB/c mice unexposed to bright light exposure received vehicle treatment (NL). Scotopic ERG was performed to evaluate the retinal function 7 d after the indicated treatments. (A) Representative electroretinograms were presented. (B and C) Amplitudes of a-wave and b-wave were plotted. Data were expressed as mean \pm S.E.M (n=5 per group). ##### Compared to that from NL, P<0.001; * compared to that from LD, P<0.05; *** compared to that from LD, P<0.001.

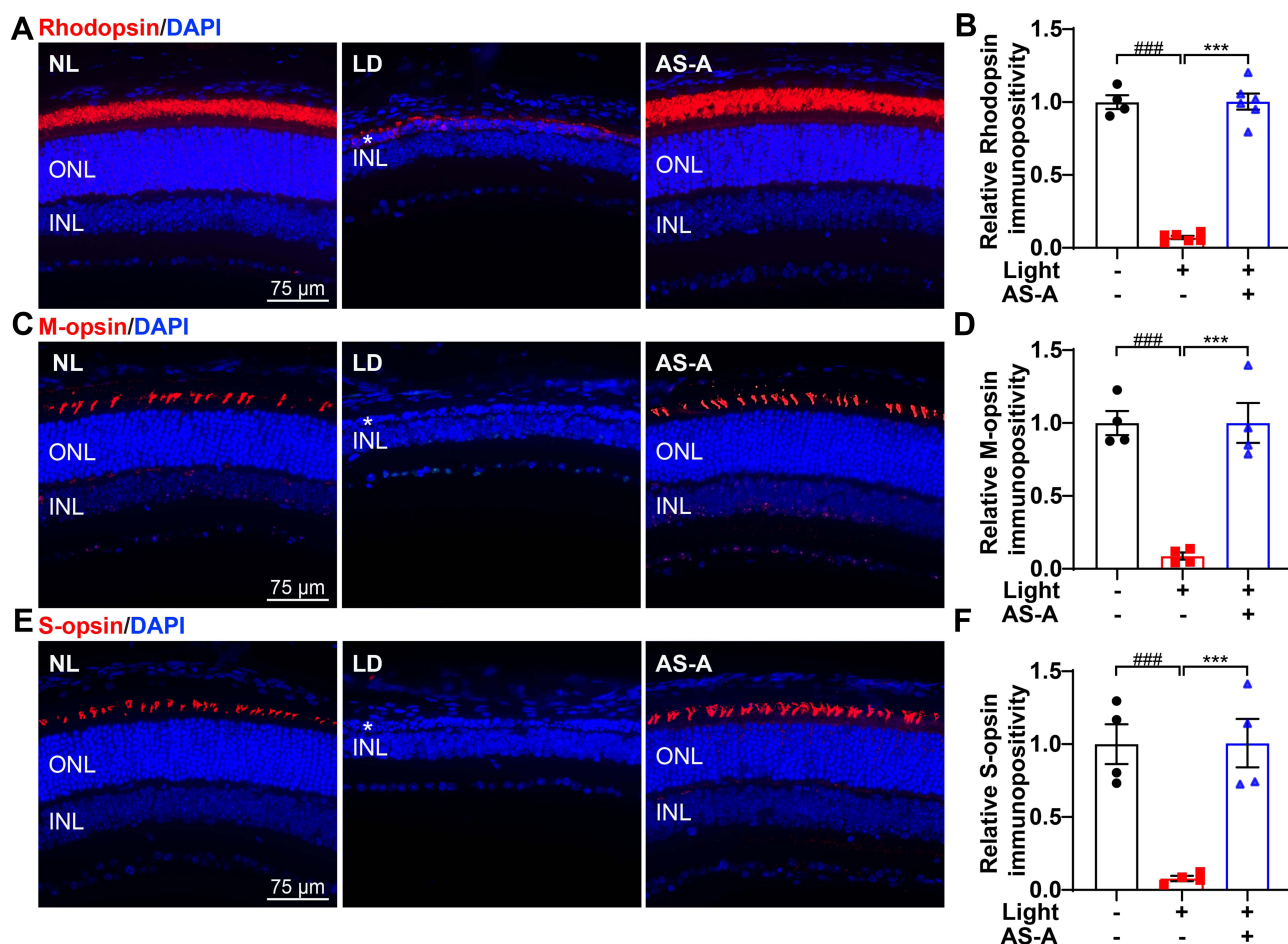


Figure 4 AS-A protects against bright light-induced obliteration of rod and cone photoreceptors. Eyes were enucleated from the indicated treatment groups 7 d after bright light exposure. (A, C, E) IHC examination of rhodopsin (A), M-opsin (C) and S-opsin (E) (in red) was performed. DAPI was counterstained to visualize the nuclei (in blue). (B, D, F) The immunopositivity of rhodopsin (B), M-opsin (D) and S-opsin (F) was quantified using ImageJ and presented as the relative immunopositivity against that from NL. White asterisk points to the impaired ONL. Data were expressed as mean±S.E.M. (n=4-6 per group). ### Compared to that from NL, P<0.001; *** compared to that from LD, P<0.001.

Abbreviations: INL, inner nuclear layer; ONL, outer nuclear layer.

controls. In contrast, the expression of rhodopsin, M-opsin and S-opsin in the light-exposed AS-A-treated retinas was found to be at similar levels to that observed in the normal controls (Figure 4A–F). In addition, IHC examination revealed marked reduction of the levels of PKC α (Figure 5A and B) and calbindin D (Figure 5C and D) in the outer plexiform layer (OPL) in the light-exposed vehicle-treated retinas compared to that from the normal controls, indicative of the impairment of the dendrites of bipolar cells and the axonal terminals of horizontal cells, respectively. However, increased immunopositivity of PKC α and calbindin D in the OPL was observed in the light-exposed AS-A-treated retinas (Figure 5A–D). The results here collectively demonstrate that AS-A treatment preserves the morphological integrity of the rod and cone photoreceptors as well as the second-order retinal neurons under photooxidative stress conditions.

AS-A Treatment Protects Against Photooxidative Stress-Induced Ultrastructural Alterations in Photoreceptors and Retinal Pigment Epithelium

Next, the retinal protective effects of AS-A at the ultrastructural level were further examined by TEM assessment. As shown in [Supplementary Figure 1](#), TEM examination revealed ultrastructural alterations in the retinal pigment epithelium (RPE) in the light-exposed vehicle-treated retinas. Although no significant morphological changes were found in the infoldings of the basal plasma membrane of the RPE, the microvilli on the apical side were noted to be significantly impaired. Meanwhile, granules with relatively uniform size and homogenous electron density were noted in the RPE in

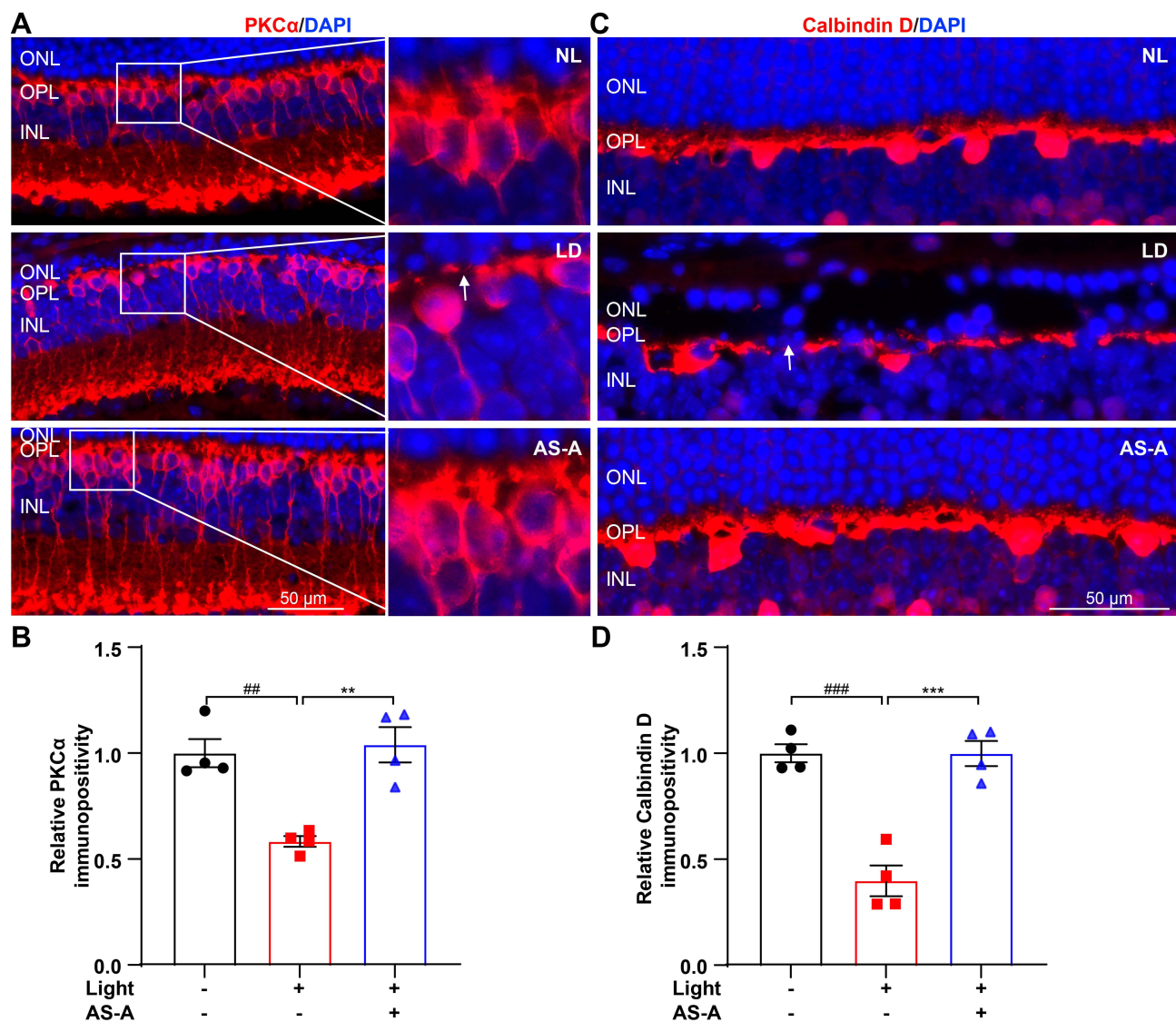


Figure 5 AS-A protects against bright light-induced morphological impairment of bipolar and horizontal cells. Eyes were enucleated from the indicated treatment groups 7 d after bright light exposure. (A and C) IHC was performed to examine the retinal expression of PKC α (A) and calbindin D (C) (in red). DAPI (in blue) was counterstained. (B and D) The immunopositivity of PKC α and calbindin D in the OPL was quantified using ImageJ and presented as the relative immunopositivity against that from NL. White arrow points to impaired dendrites of bipolar cells (A) and diminished axonal terminals of horizontal cells (C). Data were expressed as mean \pm SEM (n=4 per group). ### Compared to that from NL, P<0.01; #### compared to that from NL, P<0.001; ** compared to that from LD, P<0.01; *** compared to that from LD, P<0.001. **Abbreviations:** INL, inner nuclear layer; ONL, outer nuclear layer; OPL, outer plexiform layer.

the light-exposed vehicle-treated retinas, suggesting that bright light exposure may cause lipofuscin accumulation in the RPE.^{23,24} In the photoreceptors, the membranous discs in the OS were disorganized in the light-exposed vehicle-treated retinas (Figure 6A). In addition, the morphology of the connecting cilium was severely damaged in the light-exposed vehicle-treated retinas. Some of the photoreceptor nuclei were characterized by karyolysis and a large number of nuclei were marked by nuclear envelope breakdown and loss of euchromatin (Figure 6B). In addition, mitochondrial impairment was readily detected in the IS in the light-exposed vehicle-treated retinas. Elongated mitochondria were observed in the normal controls, whereas swollen-shaped mitochondria with disrupted cristernae were readily detected in the IS in the light-exposed vehicle-treated retinas (Figure 6C). In the photoreceptor synaptic terminals, mitochondrial impairment and loss of the electron-dense horseshoe-like synaptic ribbons were readily observed in the light-exposed vehicle-treated retinas (Figure 6D). The above-mentioned ultrastructural alterations in the indicated compartments of photoreceptors were markedly alleviated in the light-exposed AS-A-treated retinas (Supplementary Figure 1 and Figure 6). Taken

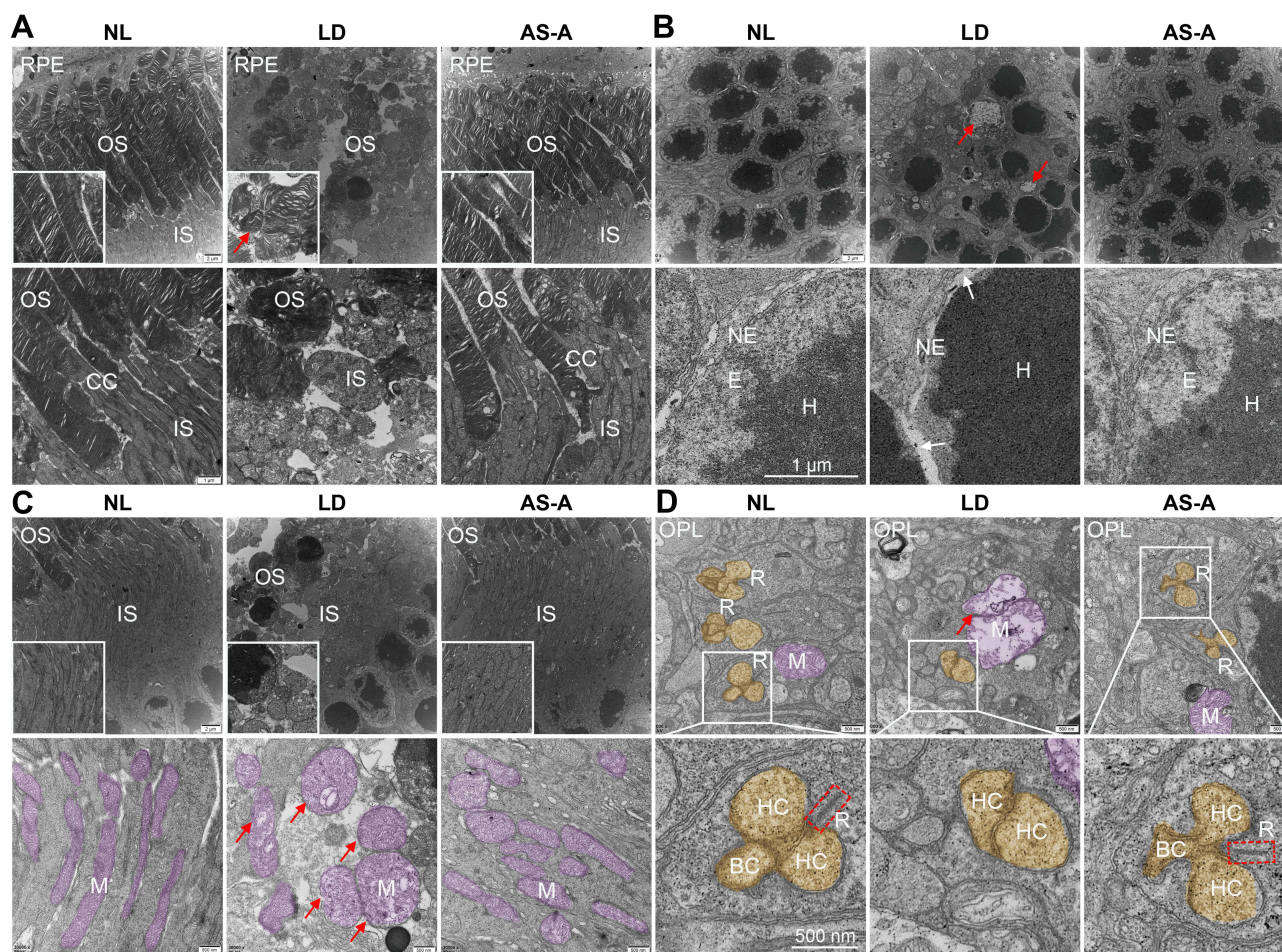


Figure 6 AS-A attenuates bright light-induced ultrastructural impairment in photoreceptors. Eyes were enucleated from the indicated treatment groups 1 d after bright light exposure, followed by processing for TEM examination. **(A–D)** Representative TEM micrographs showing the ultrastructural features of the OS and connecting cilium **(A)**, ONL **(B)**, IS **(C)** as well as mitochondria and synaptic ribbons in the OPL **(D)**. Mitochondria were highlighted in purple **(C and D)** and the dendritic tips of bipolar cells and horizontal cells were highlighted in Orange **(D)**. Red arrows point to impaired OS **(A)**, nuclei characterized by karyolysis **(B)** and swollen mitochondria **(C and D)**. White arrows point to impaired nuclear envelope **(B)**. Red squares frame synaptic ribbons in the photoreceptor synaptic terminals **(D)**. Scale bar in a and b: top panel, 2 μ m; bottom panel, 1 μ m. Scale bar in c: top panel, 2 μ m; bottom panel, 500 nm. Scale bar in d: 500 nm.

Abbreviations: BC, bipolar cell dendritic tip; CC, connecting cilium; E, euchromatin; H, heterochromatin; HC, horizontal cell dendritic tip; INL, inner nuclear layer; IS, inner segment; M, mitochondrion; NE, nuclear envelope; ONL, outer nuclear layer; OPL, outer plexiform layer; OS, outer segment; R, synaptic ribbon; RPE, retinal pigment epithelium.

together, the results here reveal that AS-A confers protection against photooxidative stress-induced impairment of the ultrastructure of photoreceptors and RPE.

In addition, IHC assessment of the expression of HSP60, lamin B1, and bassoon in the retina was performed to verify the protective effects of AS-A treatment against photooxidative stress-induced ultrastructural impairment in photoreceptor mitochondria, nuclear envelope and synaptic ribbon, respectively. HSP60 is expressed in the matrix of mitochondria, serving as a mitochondrial marker. Lamin B1 is a major structural component of the nuclear envelope and can be used as a marker for nuclear envelope. In the photoreceptors, bassoon is a major ribbon component regulating photoreceptor synapse formation. The result showed that compared to that from the normal controls, the expression of HSP60 **(Figure 7A)**, lamin B1 **(Figure 7B)** and bassoon **(Figure 7C)** was markedly reduced in photoreceptor IS, ONL and synaptic terminals, respectively, in the light-exposed vehicle-treated retinas. In contrast, AS-A treatment preserved the expression of HSP60, lamin B1 and bassoon in the photoreceptor IS, ONL and synaptic terminals, respectively, in the light-exposed retinas. These results corroborate the findings from the ultrastructural examination, further supporting the protective effects of AS-A against bright light-induced impairment of photoreceptor mitochondria, nuclear envelope and synaptic ribbon.

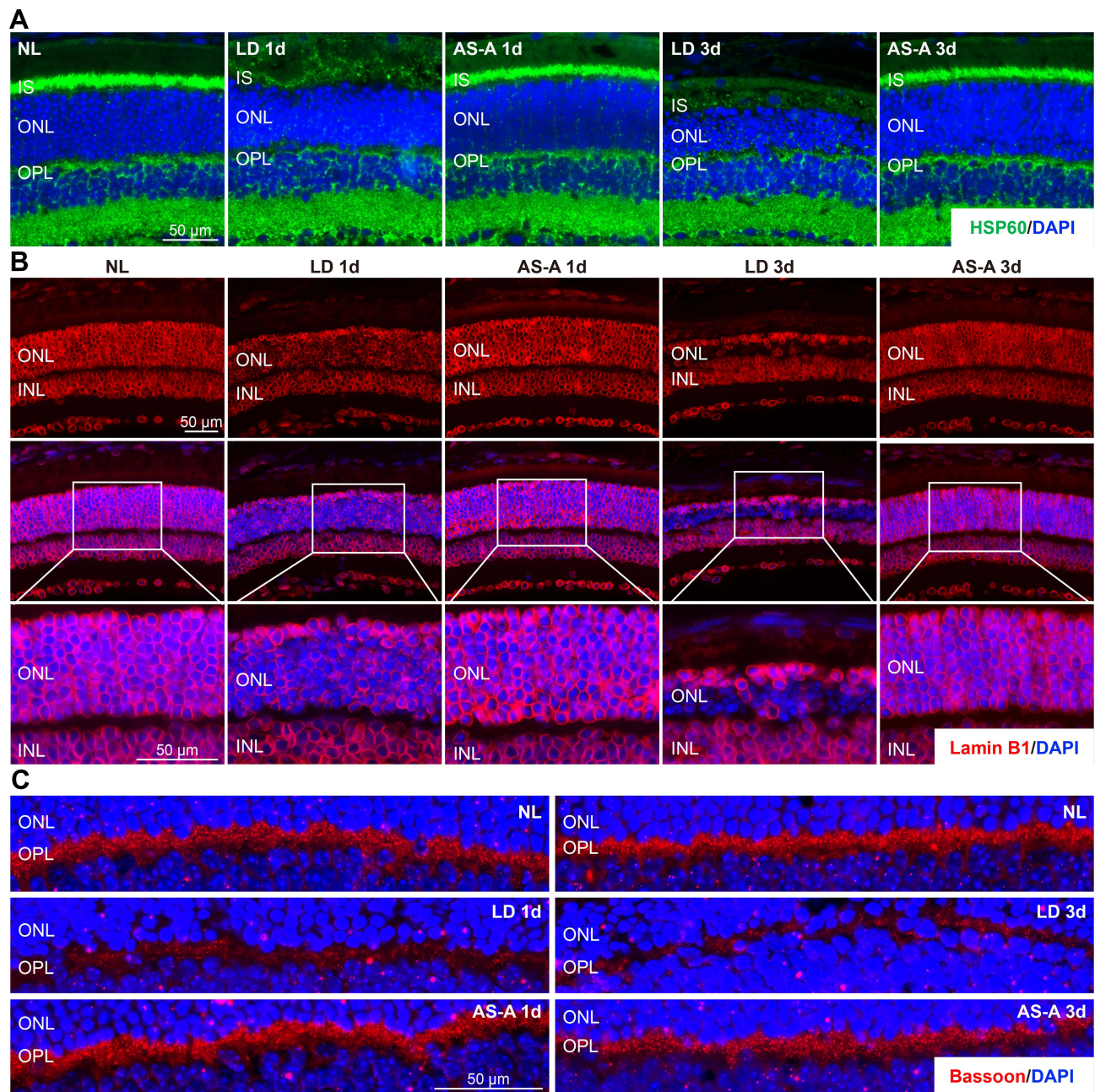


Figure 7 AS-A protects against bright light-induced impairment of mitochondria, nuclear envelope and synaptic ribbon in photoreceptors. Eyes were enucleated from the indicated treatment groups 1 d and 3 d after bright light exposure. (A–C) IHC examination was performed to detect HSP60 (in green) (A), lamin B1 (in red) (B) and bassoon (in red) (C) in the retina (n=5-6 per group). DAPI (in blue) was counterstained.

Abbreviations: INL, inner nuclear layer; IS, inner segment; ONL, outer nuclear layer; OPL, outer plexiform layer.

AS-A Treatment Alleviates Bright Light-Induced Retinal Oxidative Stress and Photoreceptor Cell Death

Heightened oxidative stress caused by overproduction of ROS and/or deficiency in the antioxidant machineries is a key mechanism in mediating photoreceptor cell death. To further assess the effect of AS-A treatment on retinal oxidative stress in the bright light-exposed retinas, a superoxide specific fluorescent probe, DHE, was administered to the mice from the indicated treatments. As shown in Figure 8A, DHE positivity was barely detected in the retinas from the normal controls. However, DHE positivity can be readily detected in the RPE and ONL in the light-exposed vehicle-treated retinas. DHE positivity in the RPE and ONL was much lower in the light-exposed AS-A-treated retinas. Next, the retinal

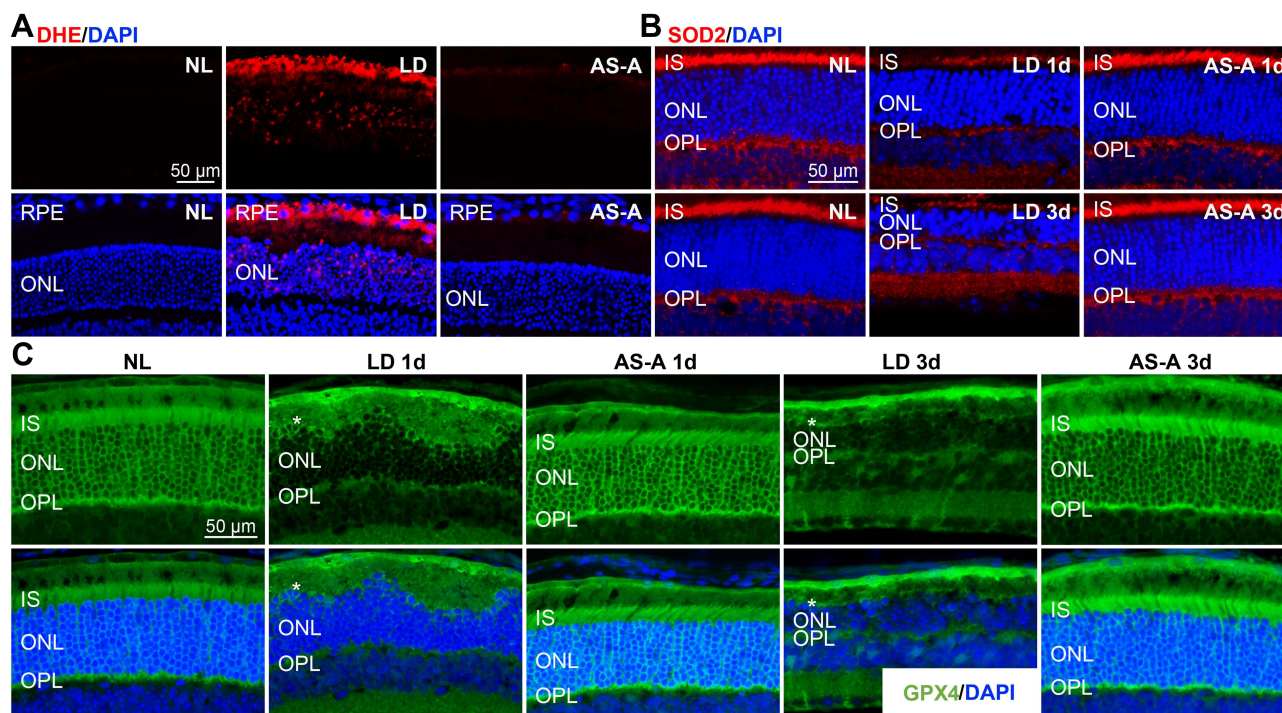


Figure 8 AS-A alleviates bright light-induced retinal oxidative stress. Dark-adapted BALB/c mice were treated with vehicle (LD) or AS-A at 100 mg/kg bw (AS-A) 30 min prior to bright light exposure. Dark-adapted BALB/c mice without bright light exposure received vehicle treatment (NL). (A) DHE was administered at 20 mg/kg bw through intraperitoneal injection 1 d after bright light exposure. Eye cups were made from the eyeballs enucleated 2 h after DHE injection, followed by cryosectioning and in situ examination of retinal ROS production. ROS signals (in red) and DAPI positivity (in blue) were examined by a fluorescence microscope (n=6 per group). (B and C) Eyeballs from the indicated treatment groups were collected 1 d and 3 d after bright light exposure. IHC examination of SOD2 (in red) (B), GPX4 (in green) (C) was then performed (n=5-6 per group). DAPI (in blue) was counterstained. White asterisks point to diminished GPX4 in the IS (C).

Abbreviations: INL, inner nuclear layer; IS, inner segment; ONL, outer nuclear layer; OPL, outer plexiform layer; RPE, retinal pigment epithelium.

expression of antioxidant enzymes SOD2 and GPX4 was examined. SOD2, expressed in the mitochondria, is the chief enzyme converting highly reactive superoxide to less reactive hydrogen peroxide, playing an important role in protecting metabolically active neurons against oxidative stress-induced damage.²⁵ GPX4 is a lipid hydroperoxidase that functions to prevent the formation of toxic lipid ROS by converting lipid hydroperoxides to lipid alcohols.²⁶ Lipid hydroperoxides are major lipid peroxidation intermediates that mediate oxidative damage and cell death. As shown in Figure 8B, SOD2 expression was readily detected in the IS and OPL in the normal controls. However, diminished SOD2 expression in the IS and OPL was observed in the light-exposed vehicle-treated retinas. In contrast, the expression of SOD2 in the IS and OPL was increased in the light-exposed AS-A-treated retinas. Moreover, the expression of GPX4 was readily detected in the IS, ONL and OPL in the normal retinas. In the light-exposed vehicle-treated retinas, the expression of GPX4 in the IS, ONL and OPL was markedly reduced. However, the expression of Gpx4 in the IS, ONL and OPL in the light-exposed AS-A-treated retinas was maintained at a comparable level to that from the normal controls (Figure 8C). TUNEL assay was further performed to confirm the impact of AS-A on photoreceptor cell death. Our previous work has demonstrated that photooxidative stress-induced photoreceptor cell death becomes readily detectable 1d after bright light exposure; the most profound changes in cell death are noted 3d after bright light exposure.⁹ Therefore, the effect of AS-A treatment on photoreceptor cell death was examined 1d and 3d after the bright light exposure. As shown in Supplementary Figure 2A and B, consistent with the previous findings, TUNEL positivity was barely detected in the retinas from the normal controls, while it was readily detected in the light-exposed vehicle-treated retinas 1d after the bright light exposure and further increased 3d after the bright light exposure. On the contrary, the bright light-induced increase in the TUNEL positivity in the ONL was not observed in the light-exposed AS-A-treated retinas. Taken together, the results here indicate that AS-A attenuates bright light-induced oxidative stress and photoreceptor cell death.

AS-A Treatment Attenuates Photooxidative Stress-Induced Necroptosis, Inflammation and Microglial Activation in the Retina

Next, RNA-seq was carried out to gain in-depth understanding of the molecular pathways implicated in the photoreceptor protective effects of AS-A. Total RNA isolated from 6 retinas from the indicated treatment groups, including the normal controls, the light-exposed vehicle-treated mice and the light-exposed AS-A-treated mice. The sequencing was performed to a mean depth of 49.90 ± 1.29 million raw reads with a genomic alignment percentage of 93.46 ± 0.18 . After normalization and elimination of the transcripts with low expression (counts <2), the data set subject to further analyses included 22,174 expressed transcripts. First, PCA demonstrated that the retinal gene expression profiles of the normal controls and the light-exposed vehicle-treated mice exhibited overt separation along principal component 1. The retinal gene expression profiles from the light-exposed AS-A-treated mice clustered to that from the normal controls (Figure 9A). Next, hierarchical clustering analysis of the DEGs revealed that AS-A treatment counteracted bright light-induced changes in the gene expression pattern in the retina, yielding a gene expression profile similar to that observed in the normal controls (Figure 9B). Furthermore, the results from GSEA of KEGG gene sets revealed that bright light exposure resulted in significant upregulation of 65 pathways and downregulation of phototransduction pathway in the retinas (Table). AS-A treatment resulted in downregulation of 64 out of 65 bright light-upregulated pathways in the retina. Meanwhile, AS-A treatment led to significant upregulation of phototransduction pathway in the light-exposed retinas (Table). Therefore, the results from the transcriptomic analyses indicate that AS-A treatment counteracts photooxidative stress-altered retinal gene expression in a broad manner.

As revealed by the results from GSEA of KEGG shown in Table, bright light exposure upregulated the molecular pathways involved in cell death, including not only “Apoptosis pathway” but also programmed necrosis such as “Necroptosis pathway” and “Ferroptosis pathway”. Necrotic cell death but not apoptosis induces neurotoxic inflammatory responses that may further aggravate photoreceptor degeneration. Consistently, GSEA of KEGG revealed that a number of pathways implicated in inflammatory responses were significantly upregulated as a result of bright light exposure, for instance, TNF signaling pathway, toll-like receptor signaling pathway, NF-kappa B signaling pathway, IL-17 signaling pathway, NOD-like receptor signaling pathway, cytokine-cytokine receptor interaction and chemokine signaling pathway (Table 1). Necroptosis is a potent inducer of inflammation.²⁷ Meanwhile, as the primary resident immune cells in the retina, microglial cells play a major role in mediating inflammatory responses in the retina.²⁸ We thus set our focus on the impact of AS-A treatment on the gene sets associated with necroptosis, microglial activation and neuroinflammation. GSEA of KEGG revealed that bright light exposure-induced upregulation of necroptosis gene set (Figure 9C) was significantly downregulated in the retinas from the light-exposed AS-A-treated mice (Figure 9D). GSEA of GO revealed that bright light exposure upregulated gene sets including microglial cell activation, monocyte chemotaxis, neuroinflammatory response, regulation of tumor necrosis factor superfamily cytokine production, and antigen processing and presentation of peptide antigen in the retina. Whereas AS-A treatment led to significant downregulation of these gene sets in the retina in the presence of bright light exposure (Figure 9E–N).

Next, real-time qPCR analysis was performed to validate the changes in the retinal expression of the representative genes from the gene sets of necroptosis, microglial activation, chemotaxis and neuroinflammation, including *Ripk1*, *Ripk3*, *Mkl1*, *Fas*, *Ccl2*, *Ccl3*, *Ccl4*, *Tlr2*, *Tlr4*, *Il1b*, *Tnf*, *Tspo* and *CD68* (Figure 10A). The results revealed that compared to that from the normal controls, bright light exposure led to significantly upregulated retinal expression of the major necroptotic regulators such as *Ripk1*, *Ripk3*, *Mkl1*, *Zbp1* and *Fas* (Figure 10B), chemokines such as *Ccl2*, *Ccl3* and *Ccl4* (Figure 10C) and proinflammatory genes such as *Il1b*, *Tnf*, *Tlr2*, *Tlr4* as well as markers of microglial activation such as *Tspo* and *CD68* (Figure 10D). In contrast, AS-A treatment resulted in significantly decreased expression of *Ripk1*, *Ripk3*, *Mkl1*, *Fas*, *Ccl2*, *Ccl3*, *Ccl4*, *Tlr2*, *Tlr4*, *Il1b*, *Tnf*, *Tspo* and *CD68* in the bright light-exposed retinas compared to that from the light-exposed vehicle-treated retinas (Figure 10B–D). IHC was also performed to examine the expression of microglial specific Iba1 in the retina. As shown in Figure 10E, the Iba1 immunopositivity was restricted to the inner retina in the normal controls. In the ONL and subretinal space, Iba1 immunopositivity was not observed in the normal controls. However, the Iba1 immunopositivity was readily observed in the ONL and subretinal space in the light-exposed vehicle-treated retinas. Meanwhile, in the light-exposed vehicle-treated retinas, ectopic Iba1 positive microglial

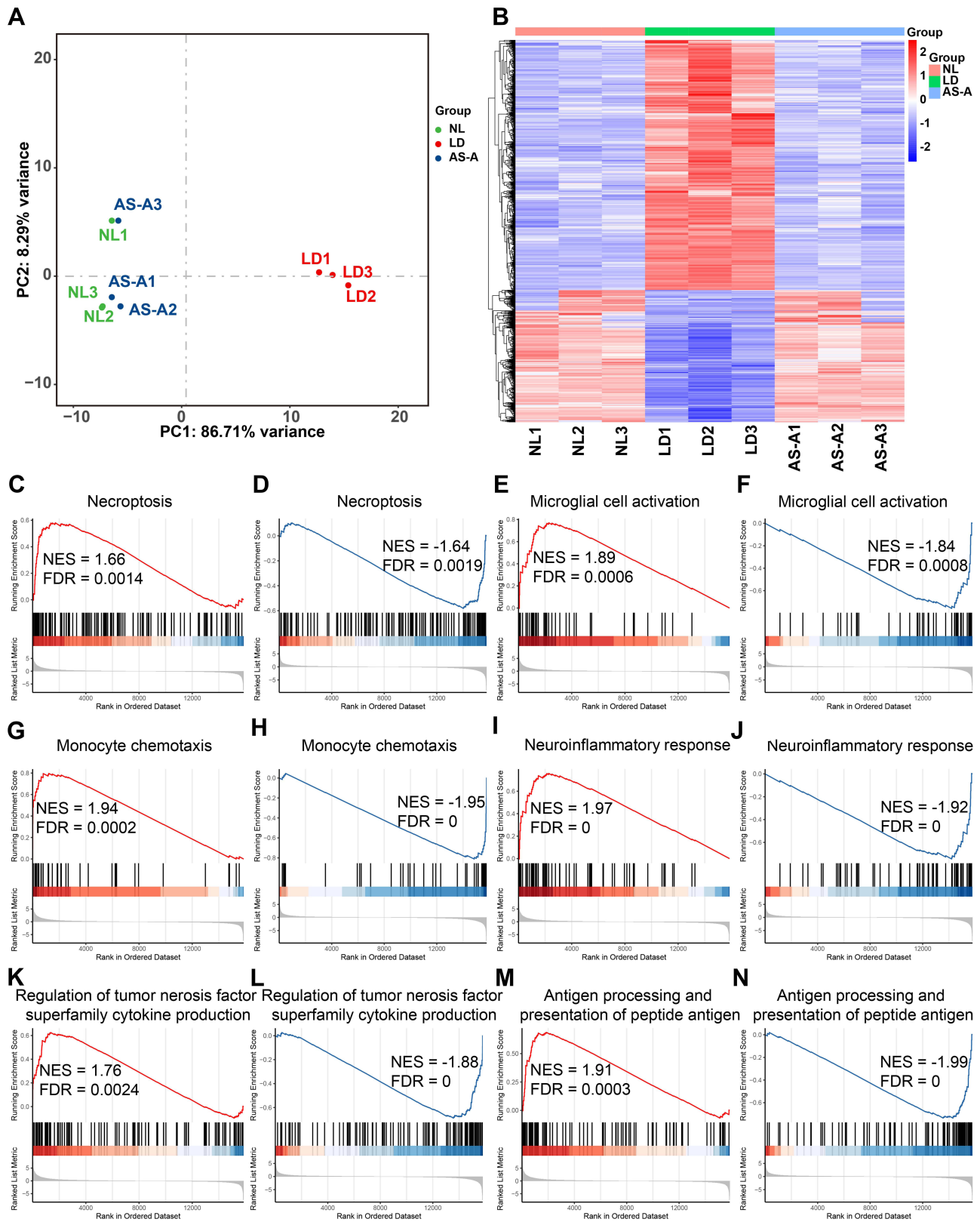


Figure 9 AS-A treatment counteracts bright light-induced alterations of the retinal gene expression profiles. Eyes were enucleated from the indicated treatment groups 1 d after bright light exposure. Total RNA was isolated from the retina, followed by RNA-seq analysis (n=3 per group). **(A)** Principal component analysis (PCA) of all data sets from NL (green), LD (red) and AS-A (blue). **(B)** Hierarchical clustering analysis of the DEGs from NL, LD and AS-A. Scale bar represents the Z score indicative of upregulation (red) and downregulation (blue) of gene expression. **(C–N)** Gene set enrichment analysis (GSEA) based on KEGG or GO gene sets.

Abbreviations: FDR, false discovery rate; NES, normalized enrichment score.

Table I The Impact of AS-A Treatment on the Gene Sets Altered by Bright Light Exposure in the Retina

Gene Sets	LD vs NL NES (FDR q-value)	AS-A vs LD NES (FDR q-value)
Phototransduction	-2.12 (0.0001)	2.15 (0.0000)
TNF signaling pathway	2.17 (0)	-2.13 (0)
Toll-like receptor signaling pathway	2.14 (0)	-2.12 (0)
Coronavirus disease - COVID-19	2.11 (0)	-2.02 (0)
NF-kappa B signaling pathway	2.11 (0)	-2.04 (0)
IL-17 signaling pathway	2.10 (0)	-2.06 (0)
NOD-like receptor signaling pathway	2.09 (0)	-2.08 (0)
Pertussis	2.05 (0)	-1.88 (0)
Osteoclast differentiation	2.04 (0)	-1.96 (0)
Influenza A	2.01 (0)	-2.05 (0)
Kaposi sarcoma-associated herpesvirus infection	2.01 (0)	-1.97 (0)
Phagosome	2.01 (0)	-1.97 (0)
Lipid and atherosclerosis	1.98 (0)	-2.01 (0)
Rheumatoid arthritis	1.98 (0)	-2.14 (0)
RIG-I-like receptor signaling pathway	1.98 (0)	-1.94 (0)
Type I diabetes mellitus	1.97 (0)	-2.04 (0)
Cytosolic DNA-sensing pathway	1.97 (0)	-1.95 (0)
Epstein-Barr virus infection	1.96 (0)	-2.19 (0)
Complement and coagulation cascades	1.96 (0)	-1.65 (0.0076)
Legionellosis	1.96 (0)	-1.89 (0)
Human cytomegalovirus infection	1.95 (0)	-1.94 (0)
Graft-versus-host disease	1.95 (0.0001)	-2.08 (0)
C-type lectin receptor signaling pathway	1.94 (0)	-1.91 (0)
Leishmaniasis	1.92 (0.0001)	-1.95 (0)
Allograft rejection	1.91 (0.0002)	-2.09 (0)
Malaria	1.91 (0.0004)	-1.91 (0)
Cytokine-cytokine receptor interaction	1.89 (0)	-2.04 (0)
Chagas disease	1.88 (0)	-1.93 (0)
Chemokine signaling pathway	1.86 (0)	-1.90 (0)
Viral myocarditis	1.84 (0.0013)	-2.07 (0)
African trypanosomiasis	1.84 (0.0021)	-1.75 (0.0029)
Alcoholic liver disease	1.83 (0)	-1.67 (0.0010)
Herpes simplex virus I infection	1.82 (0)	-1.84 (0)
Viral protein interaction with cytokine and cytokine receptor	1.81 (0.0010)	-1.95 (0)
Antigen processing and presentation	1.81 (0.0010)	-2.08 (0)
Hepatitis B	1.81 (0)	-1.85 (0)
Yersinia infection	1.80 (0.0001)	-1.87 (0)
Apoptosis	1.78 (0.0001)	-1.76 (0)
Amoebiasis	1.78 (0.0007)	-1.73 (0.0010)
Salmonella infection	1.77 (0)	-1.79 (0)
Acute myeloid leukemia	1.77 (0.0019)	-1.78 (0.0002)
JAK-STAT signaling pathway	1.76 (0.0002)	-1.96 (0)
Autoimmune thyroid disease	1.76 (0.0021)	-2.01 (0)
Human T-cell leukemia virus I infection	1.73 (0)	-2.03 (0)
Transcriptional misregulation in cancer	1.71 (0.0002)	-1.71 (0.0001)
Viral carcinogenesis	1.69 (0.0001)	-1.75 (0)
Fluid shear stress and atherosclerosis	1.69 (0.0010)	-1.60 (0.0029)
Toxoplasmosis	1.69 (0.0021)	-1.81 (0)
Tuberculosis	1.69 (0.0008)	-1.73 (0.0001)
Cellular senescence	1.68 (0.0004)	-1.66 (0.0003)

(Continued)

Table 1 (Continued).

Gene Sets	LD vs NL NES (FDR q-value)	AS-A vs LD NES (FDR q-value)
Measles	1.67 (0.0012)	-1.95 (0)
Ribosome	1.66 (0.0012)	-1.47 (0.0257)
Necroptosis	1.66 (0.0014)	-1.64 (0.0019)
Ferroptosis	1.66 (0.0184)	-1.59 (0.0332)
p53 signaling pathway	1.64(0.0235)	NE
AGE-RAGE signaling pathway in diabetic complications	1.64 (0.0031)	-1.61 (0.0035)
B cell receptor signaling pathway	1.62 (0.0190)	-1.67 (0.0043)
Human papillomavirus infection	1.60 (0.0001)	-1.64 (0)
Human immunodeficiency virus 1 infection	1.60 (0.0010)	-1.71 (0)
Natural killer cell mediated cytotoxicity	1.59 (0.0178)	-1.73 (0.0010)
Hepatitis C	1.55 (0.0120)	-1.54 (0.0090)
MicroRNAs in cancer	1.46 (0.0213)	-1.43 (0.0365)
Proteoglycans in cancer	1.46 (0.0147)	-1.61 (0.0005)
MAPK signaling pathway	1.36 (0.0326)	-1.45 (0.0052)
Pathways in cancer	1.35 (0.0086)	-1.42 (0.0008)

Abbreviations: AS-A, light-exposed AS-A-treated mice; FDR, false discovery rate; LD, light-exposed vehicle-treated mice; NES, normalized enrichment score; NL, vehicle-treated mice without light exposure.

cells were noted to be markedly enlarged. In contrast, much less Iba1 immunopositivity was observed in the ONL and subretinal space in the light-exposed AS-A-treated retinas. Taken together, these results demonstrate that AS-A treatment attenuates necroptosis, inflammation and microglial activation in the retina under photooxidative stress conditions.

AS-A Attenuates Release of HMGB1 from the Photoreceptor Nuclei Presumably Through Suppressing DNA Damage-Induced PARP Activation in the Bright Light-Exposed Retinas

Release of chromatin-associated protein HMGB1 from the photoreceptor nuclei has been noted during DNA damage-induced RIPK3-mediated photoreceptor degeneration.²⁹ As a major form of danger-associated molecular patterns (DAMPs), extracellularly released HMGB1 is equipped with potent proinflammatory properties.³⁰ Thus, it is likely that AS-A may attenuate photooxidative stress-induced DNA damage, thereby reducing release of HMGB1 from the necroptotic photoreceptor nuclei. The formation of double-strand breaks rapidly triggers the phosphorylation of the histone H2A.X, a component of the histone octamer in nucleosomes. The newly formed phosphorylated H2AX (γ H2AX) serves as a precise and sensitive marker to detect DNA double-strand breaks.³¹ To test our hypothesis, IHC was performed to examine the presence of γ H2AX and the expression pattern of HMGB1 in the retina. As shown in [Figure 11A and B](#), γ H2AX was readily detected in the ONL in the light-exposed vehicle-treated retinas. However, γ H2AX positive photoreceptor nuclei were barely detected in the light-exposed AS-A-treated retinas. These observations indicate that AS-A treatment attenuates photooxidative stress-induced DNA damage in the photoreceptors. Moreover, in the normal controls, the expression of HMGB1 was detected in the nucleated layers of the retina, including ONL, INL and the nuclei of the ganglion cells. However, an overt reduction of the HMGB1 immunopositivity in the ONL was observed in the light-exposed vehicle-treated retinas, whereas the nuclear signal of HMGB1 remained largely unaltered in the INL and the ganglion cells. In contrast, this bright light-induced reduction in the nuclear localization of HMGB1 in the ONL was not observed in the light-exposed AS-A-treated mice ([Figure 11C](#)). To further understand whether bright light-induced reduction in the nuclear immunopositivity of HMGB1 in photoreceptors is a result of decreased expression of HMGB1, real-time qPCR was performed to analyze the retinal expression of *Hmgb1*. As shown in [Supplemental Figure 3](#), no significant changes in the mRNA level of *Hmgb1* was observed in the light-exposed vehicle-treated retinas compared to that from the normal controls. In addition, the mRNA expression level of *Hmgb1* remained similar in the

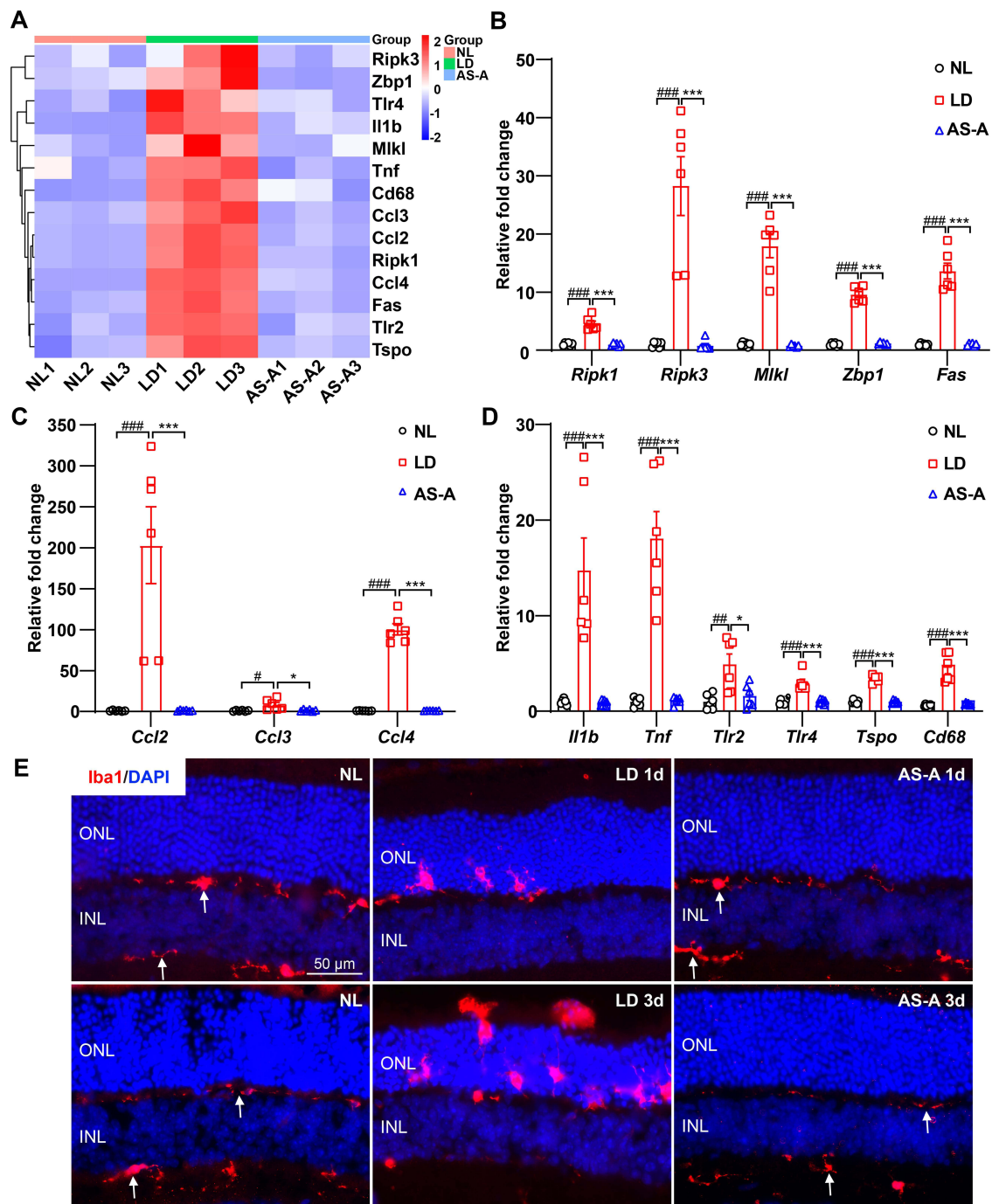


Figure 10 AS-A suppresses bright light-upregulated retinal expression of genes implicated in necroptosis and inflammation and attenuates microglial activation in the retina. **(A)** Heatmap visualization of the representative genes from the gene sets presented in Figure 9C-N. **(B–D)** Dark-adapted BALB/c mice were treated with vehicle (LD) or AS-A at 100 mg/kg bw (AS-A) 30 min before bright light exposure. Dark-adapted BALB/c mice without bright light exposure received vehicle treatment (NL). Total RNA was isolated from the indicated treatment groups 1 d after bright light exposure. Real-time qPCR was performed to verify the changes in the retinal expression of genes involved in necroptosis **(B)**, chemotaxis **(C)** and inflammation as well as microglial activation **(D)** (n=6 per group). 18S rRNA was included as the internal reference. Relative fold change was plotted against that from NL. **(E)** Eyeballs were enucleated 1 d and 3 d after the indicated treatment, followed by IHC examination of the expression of Iba1 (in red) (n = 4 per group). DAPI (in blue) was counterstained. White arrows point to resting microglia. Data were expressed as mean±S.E.M. # Compared to that from NL, P<0.05; ### compared to that from NL, P<0.01; #### compared to that from NL, P<0.001; * compared to that from LD, P<0.05; *** compared to that from LD, P<0.001. **Abbreviations:** INL, inner nuclear layer; ONL, outer nuclear layer.

light-exposed AS-A-treated retinas as that from the light-exposed vehicle-treated mice. Furthermore, it has been demonstrated that DNA damage-triggered hyperactivation of PARP is in part implicated in RIPK3-mediated photoreceptor cell death and release of nuclear HMGB1.^{29,32} Therefore, the activity of PARP was further examined by probing

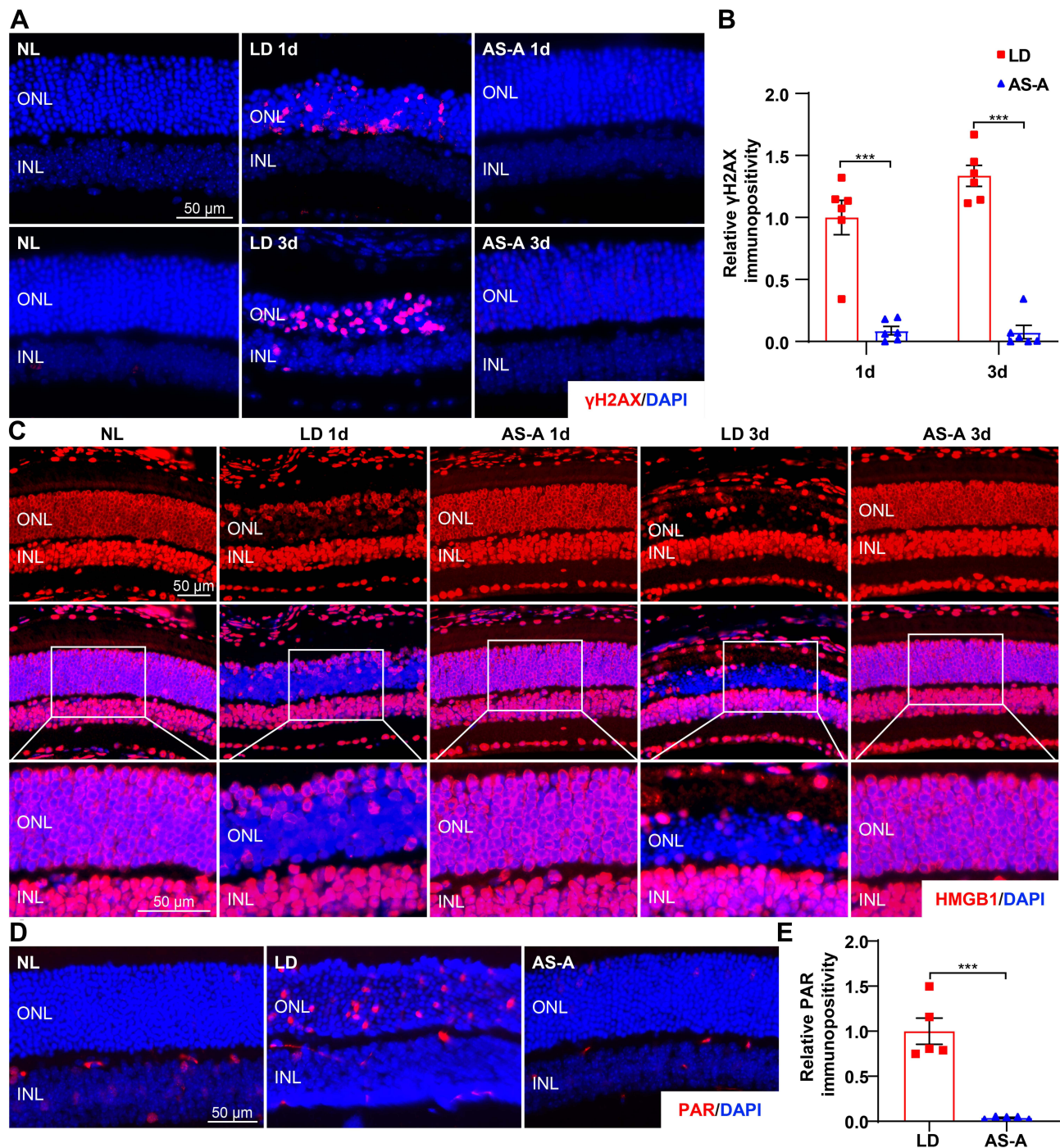


Figure 11 AS-A suppresses bright light-induced DNA damage, PARP activation and release of HMGB1 from the photoreceptor nuclei. Eyeballs were enucleated 1 d and/or 3 d after the indicated treatments. (A) IHC was performed to detect γ H2AX (in red) in the retina. DAPI (in blue) was counterstained. (B) The immunopositivity of γ H2AX in the ONL was quantified using ImageJ and presented as the relative immunopositivity against that from LD. (C) IHC was performed to detect HMGB1 (in red) in the retina. DAPI (in blue) was counterstained. (D) IHC was performed to examine PAR (in red) in the retina. DAPI (in blue) was counterstained. (E) The immunopositivity of PAR in the ONL was quantified using ImageJ and presented as the relative immunopositivity against that from LD. Data were expressed as mean \pm S.E.M (n=5-6 per group). *** Compared to that from LD, $P<0.001$.

Abbreviations: INL, inner nuclear layer; ONL, outer nuclear layer.

the presence of polymers of ADP-ribose (PAR) in the retina. As shown in Figure 11D and E, the presence of PAR was observed in the ONL in the light-exposed vehicle-treated retinas but not in the ONL in the normal controls. In contrast, the PAR immunopositivity in the ONL was not observed in the light-exposed AS-A-treated retinas. Taken together, these

results demonstrate that AS-A mitigates photooxidative stress-induced DNA damage, hyperactivation of PARP and possibly the release of HMGB1 from the photoreceptor nuclei.

The Photoreceptor Protective Effect of AS-A is in Part Mediated by Direct Mitigation of DNA Damage-Mediated Photoreceptor Degeneration

Although the results shown in Figure 11 indicate that AS-A treatment alleviates oxidative stress-induced DNA damage in the photoreceptors, it is unclear whether AS-A has a direct impact on DNA damage or the DNA damage-relieving effect of AS-A is merely a result from attenuated oxidative stress in the retina. To further address the hypothesis that AS-A may have a direct impact on DNA damage-mediated photoreceptor degeneration, MMS, a DNA alkylating agent, was adopted to selectively induce DNA damage-mediated photoreceptor degeneration.³³ OCT imaging revealed that MMS disrupted the integrity of the photoreceptor microstructure and caused subretinal edema. However, the microstructural impairment of photoreceptor and subretinal edema were remarkably attenuated in the MMS-challenged AS-A-treated retinas (Figure 12A). Measurement of the ONL thickness showed that the ONL was much thinner in the MMS-challenged vehicle-treated retinas compared to that from the normal controls. However, increased ONL thickness was observed in the MMS-challenged AS-A-treated retinas compared to that from the MMS-challenged vehicle-treated retinas (Figure 12B). Histological examination confirmed MMS-induced morphological impairment in the photoreceptor OS, IS, ONL and RPE in the vehicle-treated retinas. In contrast, the morphological integrity of OS, IS, ONL and RPE was partially preserved in the MMS-challenged AS-A-treated retinas (Figure 12C). Measurement of the number of photoreceptor rows showed that AS-A treatment resulted in increased number of photoreceptor rows compared to that from the

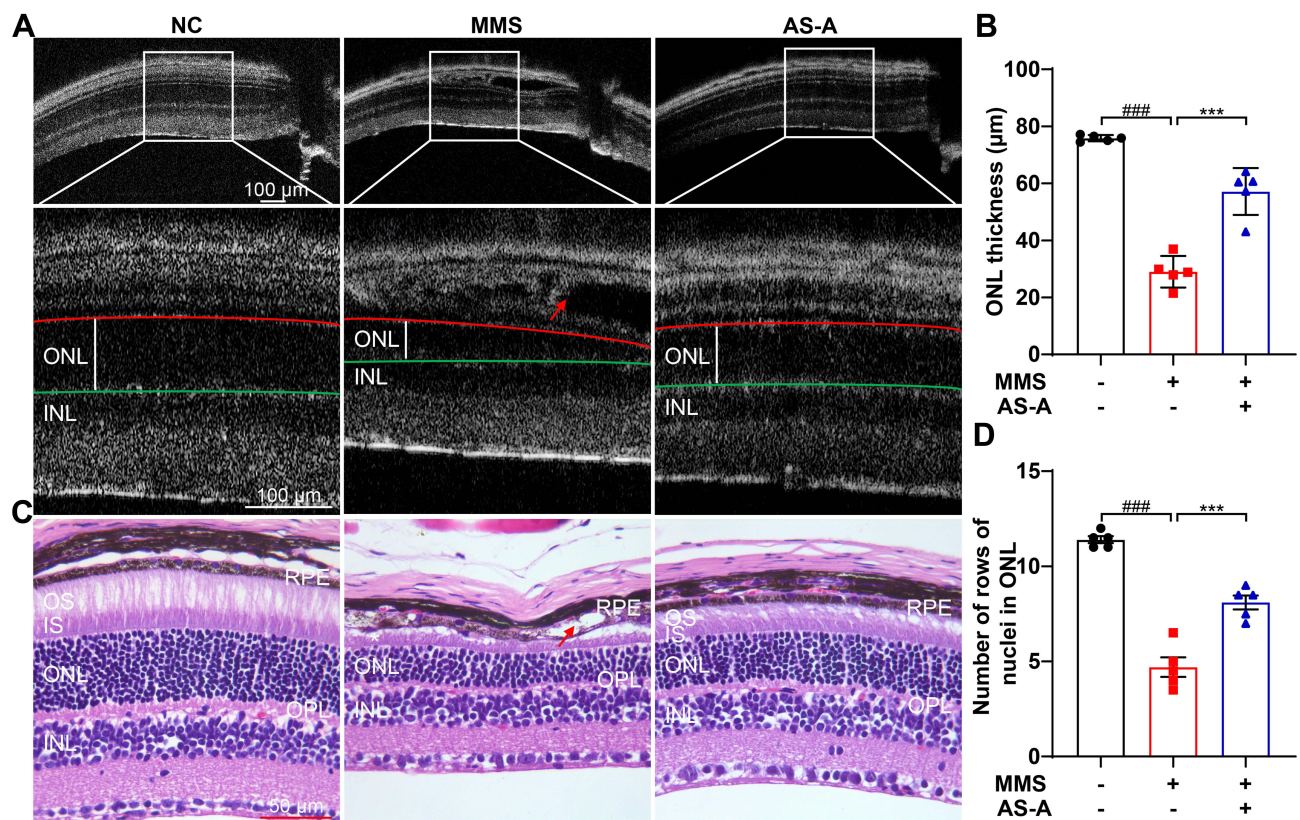


Figure 12 AS-A protects against MMS-induced retina degeneration. C57/BL6J mice were challenged by MMS at 55 mg/kg bw, followed by the treatment 0.9% saline solution (MMS) or AS-A at 100 mg/kg bw (AS-A) twice a day for 7 days. C57/BL6 mice without MMS challenge received vehicle treatment in the same manner (NC). (A) Seven days after MMS challenge, OCT imaging was performed to visualize the retinal microstructure. (B) The thickness of ONL was measured at 500 µm off the ONH. (C) Histological examination was performed by HE staining of the paraffin sections. Representative micrographs were presented showing the morphological features of the central retina. (D) The number of rows of nuclei in ONL was measured. Red arrows point to subretinal edema and damaged RPE. White asterisk points to diminished IS/OS. Data were expressed as mean±S.E.M (n=5 per group). #### Compared to that from NC, P<0.001; *** compared to that from MMS, P<0.001.

Abbreviations: INL, inner nuclear layer; IS, inner segment; ONL, outer nuclear layer; OPL, outer plexiform layer; OS, outer segment; RPE, retinal pigment epithelium.

MMS-challenged vehicle-treated retinas (Figure 12D). Taken together, these results indicate that AS-A treatment may have a direct impact on DNA damage-induced photoreceptor degeneration.

AS-A Alleviates DNA Damage-Induced Retinal Expression of Necroptotic and Proinflammatory Genes and Microglial Activation in the Retina

Next, the impact of AS-A treatment on DNA damage-induced retinal expression of genes implicated necroptosis, inflammation and microglial activation was examined by real-time qPCR analyses. The results revealed elevated expression of *Ripk1*, *Ripk3*, *Mlkl*, *Zbp1*, *Fas*, *Tnf*, *Ccl2*, *Il1b* and *CD68* in the MMS-challenged vehicle-treated retinas compared to that from the normal controls. In distinct contrast, the retinal expression of *Ripk1*, *Ripk3*, *Mlkl*, *Zbp1*, *Fas*, *Tnf*, *Ccl2*, *Il1b* and *CD68* was much lower in the MMS-challenged AS-A-treated mice compared to that from the MMS-challenged vehicle-treated mice (Figure 13A and B). In addition, IHC examination showed that Iba1 immunopositivity was detected in the ONL in the MMS-challenged vehicle-treated retinas. Less Iba1 immunopositivity was observed in the ONL in the MMS-challenged AS-A-treated retinas (Figure 13C). Taken together, these results demonstrate that AS-A treatment protects against DNA damage-induced expression of pro-necroptotic and proinflammatory genes as well as microglial activation in the retina.

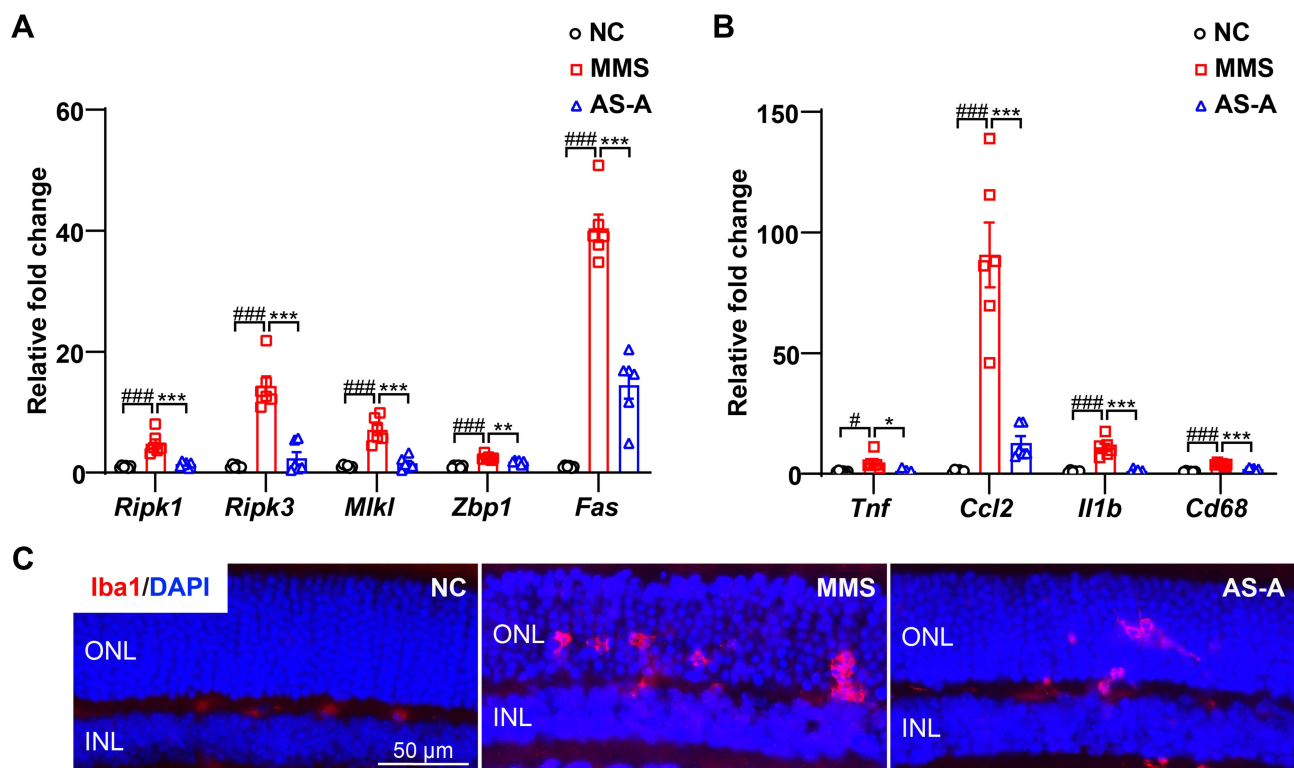


Figure 13 AS-A suppresses MMS-induced expression of necroptotic and proinflammatory genes and attenuates microglial activation in the retina. C57/BL6] mice were challenged by MMS at 55 mg/kg bw, treated by 0.9% saline solution (MMS) or AS-A at 100 mg/kg bw (AS-A). C57/BL6 mice without MMS challenge received vehicle treatment (NC). (A and B) Total RNA was isolated from the retinas collected 6 h after the indicated treatments. Real-time qPCR was then performed to analyze the expression of genes involved in necroptosis (A) and inflammatory responses as well as microglial activation (B) (n=6 per group). 18S rRNA was included as the internal reference. Relative fold change was plotted against that from NC. (C) Cryosections were made from the eye cups collected 1 d after the indicated treatments, followed by IHC examination of the expression of Iba1 (in red) in the retina (n=4 per group). DAPI (in blue) was counterstained. Data were expressed as mean±S.E.M. # Compared to that from NC, P<0.05; #### Compared to that from NC, P<0.001; * compared to that from MMS, P<0.05; ** compared to that from MMS, P<0.01; *** compared to that from MMS, P<0.001.

Discussion

In the current work, multiple lines of evidence support the pharmacological significance of AS-A in protecting against photoreceptor degeneration. Furthermore, the findings here demonstrate that AS-A mitigates necroptosis, inflammation and microglial activation in the retina in part through suppressing oxidative stress and DNA damage.

A major finding of our current work relates to the photoreceptor protective effects of AS-A. Photoreceptors are the first-order retinal neurons carrying out light-absorption and phototransduction functions essential for initiation of vision. The specialized functions of photoreceptors are supported by an exquisitely organized structure consisting of the OS, connecting cilium, IS, nucleus-containing cell body and synaptic terminal.^{34,35} The photoreceptor OS is composed of discs of folded double membranes containing essential function proteins such as rhodopsin and opsin for light absorption and phototransduction. The IS harbors a large number of mitochondria as well as Golgi and endoplasmic reticulum, where the majority of the photoreceptor metabolism and housekeeping biosynthesis take place. The connecting cilium physically connects the OS with IS. As a transitional structure between the OS and IS, connecting cilium functions as a conduit for the continual transport of proteins, membranes and small molecules. The cell body of photoreceptors accommodates the photoreceptor nucleus and transitions to the unmyelinated axon that ends with a specialized synaptic structure called ribbon synapse. The photoreceptor ribbon synapse connects with the dendritic terminals of neighboring bipolar cells and the tips of horizontal cell processes, thereby relaying phototransduction signals via the release of neurotransmitters. The morphological integrity of each of the individual photoreceptor structural compartment constitutes the essential foundation for the proper function of photoreceptors. In this work, OCT imaging (Figure 1), histological examination (Figure 2), immunohistological (Figures 4 and 7) and ultrastructural assessment (Figure 6) collectively demonstrate that AS-A treatment counteracts bright light-induced impairment of the photoreceptor OS, connecting cilium, IS, cell body and synaptic terminal. The well-maintained integrity of photoreceptors may in part contribute to the improved retinal function as a result of AS-A treatment (Figure 3).

Moreover, our work highlights the pharmacological significance of AS-A in protecting against oxidative stress-mediated photoreceptor degeneration. Photoreceptors are innately vulnerable to oxidative stress-induced damage due to high levels of oxygen exposure, high metabolic rates and high content of polyunsaturated fatty acids in the membrane of the OS. Oxidative stress, a state of imbalance between the antioxidant capacities and the amount of ROS to be tackled, plays a key role in photoreceptor cell death. Bright light exposure induces photoreceptor degeneration mainly through triggering excessive oxidative stress in the retina, recapitulating the primary pathophysiological features in patients with photoreceptor dystrophies such as age-related macular degeneration and retinitis pigmentosa.^{17,36–41} AS-A protects against bright light-induced overproduction of superoxide (Figure 8), photoreceptor cell death (Supplementary Figure 2) and loss of the functional and microstructural/morphological/ultrastructural integrity of the photoreceptors (Figures 1-4, 6 and 7), providing direct evidence supporting the pharmacological implications of AS-A in antagonizing oxidative stress-mediated photoreceptor degeneration. Furthermore, the work here demonstrates that AS-A treatment maintains the expression of antioxidant enzymes, SOD2 and GPX4, in the photoreceptors under photooxidative stress conditions (Figure 8). Antioxidant enzyme SOD2 is expressed in the mitochondrial matrix where free radicals are produced from the electron transport chain. Thus SOD2 functions as a key player to keep mitochondrial oxidative stress in check, in particularly in metabolically active neurons in the central nervous system.²⁵ It efficiently converts superoxide to less reactive hydrogen peroxide before highly active superoxide causes oxidative damages to macromolecules such as DNA, lipid and protein, preventing excessive accumulation of superoxide at the site of ATP production. Loss of SOD2 results in degenerative pathologies in neuronal tissues.²⁵ Therefore, by keeping mitochondrial oxidative stress under control, SOD2 serves as an important player in protecting against neurodegeneration. In addition to SOD2-mediated antioxidant machinery, the antioxidant enzyme GPX4 plays a critical role in the survival of photoreceptors as well. The membrane of photoreceptor outer segment contains the highest amount of polyunsaturated fatty acids in the body and is extremely susceptible to oxidative damage. Coupled with the metabolically active state, photoreceptors are innately vulnerable to lipid peroxidation under oxidative stress conditions. Meanwhile, lipid peroxidation within the photoreceptor OS membrane is associated with changes in the physical and chemical properties of the membrane and the impairment of membrane proteins, for instance, rhodopsin and opsin, which are exclusively localized in the OS membrane. As a phospholipid hydroperoxidase, GPX4 protects cells against membrane lipid peroxidation by reducing peroxidized

phospholipids in the membrane. Loss of GPX4 or inactivation of GPX4 results in elevated level of lipid peroxidation.²⁶ Conditional deletion of GPX4 in photoreceptors results in decreased number of connecting cilia and impairment of OS, followed by rapid degeneration of photoreceptors.⁴² Our work here demonstrates AS-A treatment attenuates bright light-induced reduction in the expression of SOD2 and GPX4 in the photoreceptors (Figure 8), supporting the possibility that AS-A protects against oxidative stress-induced photoreceptor degeneration in part through maintaining the expression of SOD2 and GPX4 in the photoreceptors.

Our work here also reveals that AS-A protects against oxidative stress-induced mitochondrial impairment in photoreceptors. AS-A-conferred mitochondrial protection is of significant implications in that mitochondria are not only critical regulators of cell death, but also take part in maintaining the energy and functional homeostasis of photoreceptors.⁴³ Oxidative stress instigates mitochondrial damage. Dysfunctional mitochondria in turn further promote oxidative stress and oxidant-induced cell death. Thus, mitochondria are not only the targets of oxidative stress, once impaired, dysfunctional mitochondria serve as a source of oxidative stress in the photoreceptors.⁴⁴ Our ultrastructural findings reveal that AS-A treatment preserves the morphological integrity of mitochondria in the IS and synaptic terminals of photoreceptors in the presence of bright light exposure, indicating that AS-A protects against oxidative stress-induced mitochondrial impairment in photoreceptors (Figure 6). Meanwhile, photoreceptors are the most energy-demanding cells in the body. Large amount of energy is consumed by photoreceptors to satisfy the homeostatic needs to maintain the function as well as the morphological integrity of photoreceptors. As a key player in this process, mitochondria are fundamentally required for the survival and function of the photoreceptors. In the IS, mitochondria not only generate energy to support protein synthesis and the phototransduction machinery in the adjacent OS, but also serve as a calcium store to regulate the calcium homeostasis in photoreceptors. Loss of mitochondrial integrity may directly lead to impaired function and survival of the photoreceptors. Therefore, the impact of AS-A on the integrity of photoreceptor mitochondria could be two-folded, that is preserving the homeostatic functions of mitochondria and alleviating the vicious cycle of oxidative stress centered on mitochondria, thereby promoting the survival and maintaining the function of photoreceptors under photooxidative stress conditions.

In addition to attenuating oxidative stress and mitochondrial impairment, our findings here support the notion that AS-A protects against photoreceptor degeneration in part through mitigating DNA damage. Oxidative stress can result in DNA double-strand breaks, the most damaging DNA lesions that cause lethal consequences to cells.⁴⁵ Under oxidative stress conditions, byproducts of lipid peroxidation generate etheno-DNA adducts. Etheno-DNA adducts are highly mutagenic base lesions recognized and excised by base excision repair machineries. It has been demonstrated that initiation of base excision repair induces photoreceptor degeneration in the retina.²⁹ Excessive DNA damage triggers PARP hyperactivation, which may cause bioenergetic collapse and necrosis due to exaggerated NAD⁺ consumption and depletion of ATP. PARP activation-mediated formation of PAR polymers may lead to cell death by inducing bioenergetic failure, promoting chromatin condensation and caspase-independent DNA degradation. The results here demonstrate that AS-A suppresses the formation of γ H2AX foci and PARP activation in the photoreceptor nuclei (Figure 11) and mitigates photoreceptor cell death in the bright light-exposed retinas (Supplementary Figure 2), suggesting that AS-A may protect against photoreceptor degeneration in part through ameliorating oxidative stress-induced DNA damage and PARP activation in photoreceptors. Most importantly, our results demonstrate that AS-A protects against DNA alkylating agent MMS-induced photoreceptor degeneration (Figure 12) further supporting the possibility that AS-A treatment targets DNA damage machineries in ameliorating photoreceptor degeneration.

It is also worth noting that AS-A mitigates oxidative stress and DNA damage-induced upregulation of pro-necroptotic genes and inflammatory mediators as well as microglial activation in the retina (Figures 9, 10 and 13). One of the major distinguishing features between apoptosis and necrotic cell death is that the latter can result in potent induction of inflammation. Given that inflammatory response is frequently encountered in the degenerating retina, necrotic cell death has been increasingly recognized as an important mechanism in the pathogenesis of photoreceptor degeneration.^{29,46} In this work, transcriptomic analyses reveal that necroptosis pathway is significantly upregulated in the bright light-exposed retinas (Table 1 and Figure 9). Bright light exposure results in elevated retinal expression of necroptotic regulators such as *Rip1*, *Rip3*, *Mkl1*, *Zbp1*, *Fas* as well as genes involved in both necroptosis and inflammation, for instance, *Tnf*, *Tlr2* and *Tlr4*. Death receptors such as Fas and TNF receptor family as well as TLRs are primary inducers of necroptosis.

During necroptosis, RIPK1 binds to the major necroptotic regulator RIPK3 to form a pronecrotic complex. The pronecrotic RIPK1/RIPK3 complex activates MLKL, which executes necroptotic cell death by causing membrane rupture and cell lysis. In addition to MLKL-mediated membrane disruption, multiple effector mechanisms such as mitochondrial dysfunction and formation of ROS can also be triggered to execute necroptotic cell death. Necroptosis, an inflammatory mode of programmed cell death, mimicking features of apoptosis and necrosis. It has been increasingly recognized that by promoting cell death and neuroinflammation, necroptosis plays an important player in the pathogenesis of multiple neurodegenerative diseases.^{47,48} The activation of necroptotic pathway has been documented in P23H mutation-associated photoreceptor degeneration.⁴⁹ It has also been demonstrated that necroptosis plays an important role in DNA damage-induced photoreceptor degeneration and inflammation in the retina. The expression of *Ripk1* and *Ripk3* is significantly upregulated in the retinas in the MMS-challenged mice. Genetic ablation of *Ripk3* protects against MMS-induced photoreceptor degeneration as well as retinal inflammation.²⁹ Our work here supports the notion that necroptosis is also involved in photooxidative stress-induced photoreceptor degeneration. Most importantly, the results here demonstrate that AS-A treatment suppresses photooxidative stress (Figures 9 and 10) and DNA damage-induced (Figure 13) retinal expression of necroptotic regulators and proinflammatory genes and microglial activation, supporting the pharmacological potentials of AS-A in alleviating oxidative stress and DNA damage-induced necroptosis and inflammation in the retina.

Furthermore, our results also suggest that AS-A suppresses photoreceptor degeneration-associated retinal inflammation possibly through mitigating extracellular release of HMGB1 from the photoreceptors. Extracellular HMGB1 serves as a major type of DAMPs and triggers potent inflammatory responses in immune cells such as microglia.^{30,50} It has been demonstrated that DNA damage-induced PARP activation is responsible for HMGB1 dislocation from nucleus to cytoplasm. HMGB1 extracellular release can subsequently take place when the membrane integrity is impaired.³² During MMS-induced DNA damage-mediated photoreceptor degeneration, activation of PARP and nuclear dislocation of HMGB1 have been documented.²⁹ Our results here further demonstrate that while the retinal expression of *Hmgb1* is unaltered by bright light exposure (Supplemental Figure 3), photooxidative stress induces PARP activation, MLKL upregulation and HMGB1 nuclear dislocation as well as microglial activation and inflammation in the retina (Figures 10 and 11). Thus, it is possible that hyperactivation of PARP coupled with MLKL-mediated disruption of membrane integrity might cause extracellular release of HMGB1 during photooxidative stress-induced photoreceptor degeneration. Further studies are required to verify if extracellular HMGB1 release from necrotic photoreceptors indeed takes place under photooxidative stress conditions.

Lastly, it is worth pointing out that TUNEL positivity in photoreceptors from the light-exposed mice (Supplemental Figure 2) is interpreted here as an in situ indicator of photoreceptor cell death in general. It has been demonstrated that not only apoptotic cells are labeled positive by TUNEL, necrotic cells could also be stained TUNEL positive.^{51–53} The form of photooxidative stress-induced photoreceptor cell death is clearly not restricted to apoptosis as mitochondrial swelling, a feature characterizing necrosis,⁵⁴ is readily observed in photoreceptors from the bright light-exposed retinas (Figure 6). Moreover, as discussed above, our transcriptomic analyses reveal that necroptosis pathway and pathways closely related to inflammatory responses are upregulated in the bright light-exposed retinas (Table 1 and Figure 9). Our work here thus implies heterogeneity in photoreceptor cell death in the bright light-exposed retinas. Future studies are necessary to elucidate the forms of photoreceptor cell death during the course of photooxidative stress-induced photoreceptor degeneration.

Conclusions

In summary, the work here demonstrates for the first time the pharmacological significance of AS-A in attenuating bright light-induced and DNA alkylating agent MMS-induced photoreceptor degeneration. Furthermore, our work supports the notion that AS-A protects against photoreceptor degeneration in part through alleviating oxidative stress and DNA damage-mediated necroptosis and inflammation (Figure 14). Thus, the findings here provide novel experimental evidence supporting further exploration of the therapeutic value of AS-A, alone or in combination of other therapeutic agents, in the treatment of photoreceptor degenerative diseases.

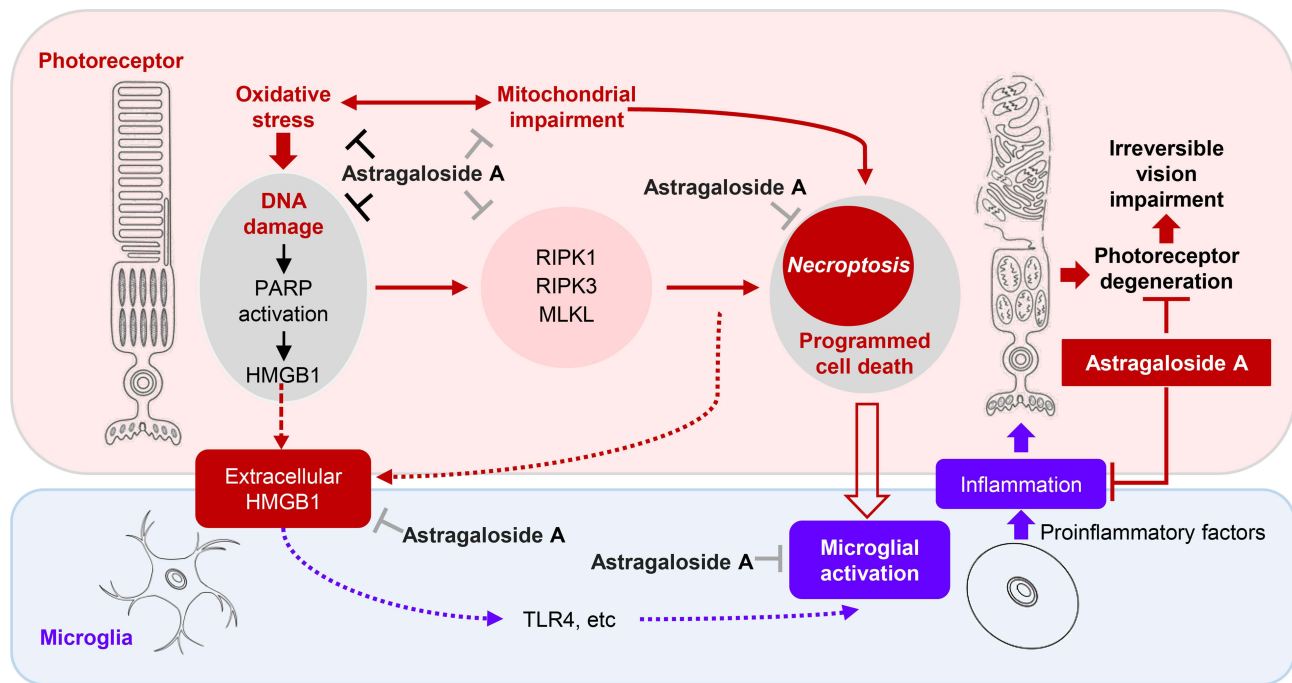


Figure 14 AS-A protects against oxidative stress and DNA damage-mediated photoreceptor degeneration in part through alleviating necroptosis and inflammation. The findings here provide direct evidence supporting that AS-A treatment attenuates the sequence of interconnected mechanistic events that mediate or aggravate photoreceptor degeneration. AS-A suppresses oxidative stress-induced mitochondrial impairment in photoreceptors. AS-A decreases oxidative stress and DNA damage-mediated retinal expression of necroptotic genes as well as the nuclear dislocation of HMGB1 from photoreceptors, which may in part contribute to its effect on alleviating neurotoxic microglial activation and retinal inflammation.

Abbreviations

AS-A, astragaloside A; DAMPs, danger-associated molecular patterns; DAPI, 4',6-diamidino-2-phenylindole; DEGs, differentially expressed genes; DHE, dihydroethidium; ERG, electroretinography; FDR, false discovery rate; GO, Gene Ontology; GPX4, glutathione peroxidase 4; GSEA, gene set enrichment analysis; HE, hematoxylin and eosin; HMGB1, high mobility group box 1; HSP60, heat shock protein 60; Iba1, ionized calcium binding adaptor molecule 1; IHC, immunohistochemistry; IS, inner segment; KEGG, Kyoto encyclopedia of genes and genomes; MMS, methyl methanesulfonate; NES, normalized enrichment score; OCT, optical coherence tomography; ONL, outer nuclear layer; OPL, outer plexiform layer; OS, outer segment; γ H2AX, Phosphorylated H2AX; PAR, polymers of ADP-ribose; PARP, poly (ADP-ribose) polymerase; PCA, principal component analysis; PKC α , protein kinase C α ; ROS, reactive oxygen species; RPE, retinal pigment epithelium; qPCR, quantitative PCR; S.E.M, standard error of mean; TEM, transmission electron microscopy; TUNEL, TdT-mediated dUTP nick-end labeling.

Acknowledgments

This work was supported by the National Natural Science Foundation of China (81673790, Y.C), Program of Shanghai Academic/Technology Research Leader (19XD1403700, Y.C) and the Science Foundation of Yueyang Hospital of Integrated Traditional Chinese and Western Medicine, Shanghai University of Traditional Chinese Medicine (2019YYZ02, Y.C). We thank An Yi-An Zhang for helping with illustrating Figure 14. We thank the research staff at the Clinical Research Institute of Integrative Medicine, Shanghai Academy of Traditional Chinese Medicine for their helpful discussion and technical support.

Disclosure

The authors report no conflicts of interest in this work.

References

1. Molday RS, Moritz OL. Photoreceptors at a glance. *J Cell Sci.* 2015;128:4039–4045.
2. Curcio CA, Medeiros NE, Millican CL. Photoreceptor loss in age-related macular degeneration. *Invest Ophthalmol Vis Sci.* 1996;37:1236–1249.
3. Wright AF, Chakarova CF, Abd El-Aziz MM, Bhattacharya SS. Photoreceptor degeneration: genetic and mechanistic dissection of a complex trait. *Nat Rev Genet.* 2010;11:273–284.
4. Nag TC. Pathogenic mechanisms contributing to the vulnerability of aging human photoreceptor cells. *Eye.* 2021;35:2917–2929.
5. Marfany G. The Relevance of Oxidative Stress in the Pathogenesis and Therapy of Retinal Dystrophies. *Antioxidants.* 2020;9:347.
6. Cuenca N, Fernández-Sánchez L, Campello L, et al. Cellular responses following retinal injuries and therapeutic approaches for neurodegenerative diseases. *Prog Retin Eye Res.* 2014;43:17–75.
7. Zhang J, Wu C, Gao L, Du G, Qin X. Astragaloside IV derived from *Astragalus membranaceus*: a research review on the pharmacological effects. *Adv Pharmacol.* 2020;87:89–112.
8. Costa IM, Lima FOV, Fernandes LCB, et al. Astragaloside IV Supplementation Promotes A Neuroprotective Effect in Experimental Models of Neurological Disorders: a Systematic Review. *Curr Neuropharmacol.* 2019;17:648–665.
9. Bian M, Du X, Cui J, et al. Celastrol protects mouse retinas from bright light-induced degeneration through inhibition of oxidative stress and inflammation. *J Neuroinflammation.* 2016;13:50.
10. Chen Y, Okano K, Maeda T, et al. Mechanism of all-trans-retinal toxicity with implications for stargardt disease and age-related macular degeneration. *J Biol Chem.* 2012;287:5059–5069.
11. Bolger AM, Lohse M, Usadel B. Trimmomatic: a flexible trimmer for Illumina sequence data. *Bioinformatics.* 2014;30:2114–2120.
12. Kim D, Langmead B, Salzberg SL. HISAT: a fast spliced aligner with low memory requirements. *Nat Methods.* 2015;12:357–360.
13. Trapnell C, Williams BA, Pertea G, et al. Transcript assembly and quantification by RNA-Seq reveals unannotated transcripts and isoform switching during cell differentiation. *Nat Biotechnol.* 2010;28:511–515.
14. Anders S, Pyl PT, Huber W. HTSeq—a Python framework to work with high-throughput sequencing data. *Bioinformatics.* 2015;31:166–169.
15. Love MI, Huber W, Anders S. Moderated estimation of fold change and dispersion for RNA-seq data with DESeq2. *Genome Biol.* 2014;15:550.
16. Wu T, Hu E, Xu S, et al. clusterProfiler 4.0: a universal enrichment tool for interpreting omics data. *Innovation.* 2021;2:100141.
17. Organisciak DT, Vaughan DK. Retinal light damage: mechanisms and protection. *Prog Retin Eye Res.* 2010;29:113–134.
18. Chen Y, Palczewska G, Masuho I, et al. Synergistically acting agonists and antagonists of G protein-coupled receptors prevent photoreceptor cell degeneration. *Sci Signal.* 2016;9:ra74.
19. Leinonen H, Pham NC, Boyd T, Santos J, Palczewski K, Vinberg F. Homeostatic plasticity in the retina is associated with maintenance of night vision during retinal degenerative disease. *Elife.* 2020;9:e59422.
20. Pfeiffer RL, Marc RE, Jones BW. Persistent remodeling and neurodegeneration in late-stage retinal degeneration. *Prog Retin Eye Res.* 2020;74:100771.
21. Samardzija M, Todorova V, Gougoulakis L, et al. Light stress affects cones and horizontal cells via rhodopsin-mediated mechanisms. *Exp Eye Res.* 2019;186:107719.
22. Sudharsan R, Simone KM, Anderson NP, Aguirre GD, Beltran WA. Acute and Protracted Cell Death in Light-Induced Retinal Degeneration in the Canine Model of Rhodopsin Autosomal Dominant Retinitis Pigmentosa. *Invest Ophthalmol Vis Sci.* 2017;58:270–281.
23. Katz ML. Potential role of retinal pigment epithelial lipofuscin accumulation in age-related macular degeneration. *Arch Gerontol Geriatr.* 2002;34:359–370.
24. Kennedy CJ, Rakoczy PE, Constable IJ. Lipofuscin of the retinal pigment epithelium: a review. *Eye.* 1995;9:763–771.
25. Flynn JM, Melov S. SOD2 in mitochondrial dysfunction and neurodegeneration. *Free Radic Biol Med.* 2013;62:4–12.
26. Maiorino M, Conrad M, Ursini F. GPx4, Lipid Peroxidation, and Cell Death: discoveries, Rediscoveries, and Open Issues. *Antioxid Redox Signal.* 2018;29:61–74.
27. Pasparakis M, Vandenabeele P. Necroptosis and its role in inflammation. *Nature.* 2015;517:311–320.
28. Rashid K, Akhtar-Schaefer I, Langmann T. Microglia in Retinal Degeneration. *Front Immunol.* 2019;10:1975.
29. Allocca M, Corrigan JJ, Mazumder A, Fake KR, Samson LD. Inflammation, necrosis, and the kinase RIP3 are key mediators of AAG-dependent alkylation-induced retinal degeneration. *Sci Signal.* 2019;12:eaau9216.
30. Lotze MT, Tracey KJ. High-mobility group box 1 protein (HMGB1): nuclear weapon in the immune arsenal. *Nat Rev Immunol.* 2005;5:331–342.
31. Kuo LJ, Yang LX. Gamma-H2AX - a novel biomarker for DNA double-strand breaks. *Vivo.* 2008;22:305–309.
32. Ditsworth D, Zong WX, Thompson CB. Activation of poly(ADP)-ribose polymerase (PARP-1) induces release of the pro-inflammatory mediator HMGB1 from the nucleus. *J Biol Chem.* 2007;282:17845–17854.
33. Meira LB, Moroski-Erkul CA, Green SL, et al. Aag-initiated base excision repair drives alkylation-induced retinal degeneration in mice. *Proc Natl Acad Sci U S A.* 2009;106:888–893.
34. Perkins BD, Fadool JM. Photoreceptor structure and development analyses using GFP transgenes. *Methods Cell Biol.* 2010;100:205–218.
35. Baehr W, Hanke-Gogokhia C, Sharif A, et al. Insights into photoreceptor ciliogenesis revealed by animal models. *Prog Retin Eye Res.* 2019;71:26–56.
36. Organisciak DT, Darrow RM, Barsalou L, et al. Light history and age-related changes in retinal light damage. *Invest Ophthalmol Vis Sci.* 1998;39:1107–1116.
37. Beatty S, Koh H, Phil M, Henson D, Boulton M. The role of oxidative stress in the pathogenesis of age-related macular degeneration. *Surv Ophthalmol.* 2000;45:115–134.
38. Winkler BS, Boulton ME, Gottsch JD, Sternberg P. Oxidative damage and age-related macular degeneration. *Mol Vis.* 1999;5:32.
39. Zarbin MA. Current concepts in the pathogenesis of age-related macular degeneration. *Arch Ophthalmol.* 2004;122:598–614.
40. Komeima K, Rogers BS, Lu L, Campochiaro PA. Antioxidants reduce cone cell death in a model of retinitis pigmentosa. *Proc Natl Acad Sci U S A.* 2006;103:11300–11305.
41. Shen J, Yang X, Dong A, et al. Oxidative damage is a potential cause of cone cell death in retinitis pigmentosa. *J Cell Physiol.* 2005;203:457–464.
42. Ueta T, Inoue T, Furukawa T, et al. Glutathione peroxidase 4 is required for maturation of photoreceptor cells. *J Biol Chem.* 2012;287:7675–7682.
43. Wright AF, Jacobson SG, Cideciyan AV, et al. Lifespan and mitochondrial control of neurodegeneration. *Nat Genet.* 2004;36:1153–1158.

44. Lin MT, Beal MF. Mitochondrial dysfunction and oxidative stress in neurodegenerative diseases. *Nature*. 2006;443:787–795.
45. Cooke MS, Evans MD, Dizdaroglu M, Lunec J. Oxidative DNA damage: mechanisms, mutation, and disease. *FASEB J*. 2003;17:1195–1214.
46. Sato K, Li S, Gordon WC, et al. Receptor interacting protein kinase-mediated necrosis contributes to cone and rod photoreceptor degeneration in the retina lacking interphotoreceptor retinoid-binding protein. *J Neurosci*. 2013;33:17458–17468.
47. Yuan J, Amin P, Ofengeim D. Necroptosis and RIPK1-mediated neuroinflammation in CNS diseases. *Nat Rev Neurosci*. 2019;20:19–33.
48. Dhuriya YK, Sharma D. Necroptosis: a regulated inflammatory mode of cell death. *J Neuroinflammation*. 2018;15:199.
49. Kakavand K, Jobling AI, Greferath U, Vessey KA, de Jongh RU, Fletcher EL. Photoreceptor Degeneration in Pro23His Transgenic Rats (Line 3) Involves Autophagic and Necroptotic Mechanisms. *Front Neurosci*. 2020;14:581579.
50. Scaffidi P, Misteli T, Bianchi ME. Release of chromatin protein HMGB1 by necrotic cells triggers inflammation. *Nature*. 2002;418:191–195.
51. de Torres C, Munell F, Ferrer I, Reventós J, Macaya A. Identification of necrotic cell death by the TUNEL assay in the hypoxic-ischemic neonatal rat brain. *Neurosci Lett*. 1997;230:1–4.
52. Grasl-Kraupp B, Ruttkay-Nedecky B, Koudelka H, Bukowska K, Bursch W, Schulte-Hermann R. In situ detection of fragmented DNA (TUNEL assay) fails to discriminate among apoptosis, necrosis, and autolytic cell death: a cautionary note. *Hepatology*. 1995;21:1465–1468.
53. Napoletano F, Gibert B, Yacobi-Sharon K, et al. p53-dependent programmed necrosis controls germ cell homeostasis during spermatogenesis. *PLoS Genet*. 2017;13:e1007024.
54. Nieminen AL. Apoptosis and necrosis in health and disease: role of mitochondria. *Int Rev Cytol*. 2003;224:29–55.

Journal of Inflammation Research

Dovepress

Publish your work in this journal

The Journal of Inflammation Research is an international, peer-reviewed open-access journal that welcomes laboratory and clinical findings on the molecular basis, cell biology and pharmacology of inflammation including original research, reviews, symposium reports, hypothesis formation and commentaries on: acute/chronic inflammation; mediators of inflammation; cellular processes; molecular mechanisms; pharmacology and novel anti-inflammatory drugs; clinical conditions involving inflammation. The manuscript management system is completely online and includes a very quick and fair peer-review system. Visit <http://www.dovepress.com/testimonials.php> to read real quotes from published authors.

Submit your manuscript here: <https://www.dovepress.com/journal-of-inflammation-research-journal>